

Review of Top Quark Physics

Dhiman Chakraborty, Northern Illinois University

Jacobo Konigsberg, University of Florida

David Rainwater, DESY

KEYWORDS: top quark, heavy fermion, Standard Model, Tevatron, LHC, top properties

ABSTRACT: We present an overview of Top Quark Physics - from what has been learned so far at the Tevatron, to the searches that lie ahead at present and future colliders. We summarize the richness of the measurements and discuss their possible impact on our understanding of the Standard Model by pointing out their key elements and limitations. When possible, we discuss how the top quark may provide a connection to new or unexpected physics. The literature on many of the topics we address is sizeable. We've attempted to consolidate the most salient points and still give the reader a complete, coherent overview. For more details the reader is kindly referred to the corresponding seminal papers.

CONTENTS

Overview	2
<i>Theoretical perspective</i>	4
<i>The Experimental arena</i>	5
Top Quark Production	11
<i>Pair production</i>	11
<i>Single top production</i>	20
<i>Sensitivity to New Physics</i>	27

Top Quark Decays	31
<i>Standard Model top quark decays</i>	32
<i>Top quark decays beyond the Standard Model</i>	34
Top Quark Properties	41
<i>Mass</i>	41
<i>Spin</i>	52
<i>Charge</i>	56
<i>Gauge couplings</i>	57
<i>Lifetime and V_{tb}</i>	60
<i>Yukawa coupling</i>	63
Summary	65

1 Overview

The discovery of the top quark at Fermilab's $p\bar{p}$ collider Tevatron in 1995 by the CDF and DØ collaborations (1) suggested the direct experimental confirmation of the three-generation structure of the Standard Model (SM) and opened up the new field of top quark physics. Several properties of the top quark were studied at the Tevatron during its first run. These include measurement of $t\bar{t}$ pair production cross section (2) and kinematical properties (3,4,5,6), top mass (7,4,5,6,8), tests of the SM via studies of W helicity in top decays (9) and spin correlations in $t\bar{t}$ production (10), searches for electroweak production of single top quarks (11,12) and for exotic decays of top such as charged Higgs (14,13), and flavor-changing neutral currents (15), etc. Precision of most of these measurements are limited by statistical uncertainties because of the small size of the data samples collected so far at the Tevatron (Run 1). Run 2, currently underway, will increase the

statistics by approximately two orders of magnitude while the Large Hadron Collider (LHC) and will be a true top factory, producing tens of millions of top quarks every year (see Table 1). The next e^+e^- Linear Collider (LC) would also have sufficient energy to produce top quarks, and be ideally suited to precision studies of many top quark properties.

The most striking observed feature that sets the top quark apart from the other quarks is its very large mass. Weighing in at 174.3 ± 5.1 GeV (7), it is about 35 times heavier than the next heaviest quark, bottom (b), and is the heaviest elementary particle known. The top quark, W and Higgs boson all contribute to radiative terms in theoretical calculations of many observables that have been measured with good precision by LEP, SLC and low-energy neutrino scattering experiments. Hence, precision measurement of m_t and M_W constrain the mass of the SM Higgs boson, as shown in Fig. 1.

The vast swath of phase space available to the decay of such a heavy quark gives it an extremely short lifetime, about 4×10^{-25} s in the SM, $\mathcal{O}(10)$ times shorter than the characteristic hadronization time of QCD, $\tau_{had} \approx 28 \times 10^{-25}$ s. As a result, the decay of top quarks offers a unique window on the properties of a bare quark free from the long-range effects of QCD, such as confinement.

The large mass of the top quark takes on even greater significance in various extensions of the SM as particle spectra and flavor- or mass-dependent couplings beyond the SM are contemplated: most such particles are experimentally constrained to be heavier than all other known fermions, but some may yet be lighter than the top quark and can appear on-shell in its decays. The top quark mass is also very close to the energy scale of Electroweak Symmetry Breaking (EWSB). Indeed, its Yukawa coupling is curiously close to 1. This raises the possibility

that perhaps there is more to it than its mass being generated by the SM Higgs mechanism in the same way as postulated with other fermions.

1.1 Theoretical perspective

In the SM, the top quark is defined as the weak isospin partner of the bottom quark. As such, it is a spin- $\frac{1}{2}$ fermion of electric charge $+\frac{2}{3}$ and transforms as a color anti-triplet under the $SU(3)$ gauge group of strong interactions. None of these quantum numbers have yet been directly measured, although a large amount of indirect evidence supports the SM assignments. Precision measurements of the $Z \rightarrow b\bar{b}$ partial width and forward-backward asymmetry at LEP (16), of B^0 - \bar{B}^0 mixing, and limits on FCNC decays of B mesons require the existence of a particle with $T_3 = \frac{1}{2}$, $Q = \frac{2}{3}$ and mass near 170 GeV, consistent with the direct measurements by the Tevatron experiments (17). The Tevatron $t\bar{t}$ production cross section measurements are also consistent with theoretical calculations for a particle with these attributes. While Tevatron Run 2 will make more stringent tests, well enough to remove any doubt that this is not the SM top quark, direct measurement of some of the top quark quantum numbers will be possible only at the LHC and a LC.

The most pressing challenge in particle theory is to explain the dynamics behind mass generation, which has two aspects: EWSB, whereby the W and Z bosons acquire mass; and flavor symmetry breaking (FSB), which splits the fermions into generations hierarchically arranged in mass. The SM accommodates both by postulating a fundamental scalar field, the Higgs. But this does not satisfactorily explain the dynamics, and the Higgs sector runs into problems at high energy scales. One well-studied new physics explanation for this is *technicolor*

(TC), which postulates a new strong gauge interaction at the TeV scale. The top quark often plays a central role in this class of models. Another possibility is *supersymmetry* (SUSY), a new global space-time symmetry. The minimal SUSY model (MSSM) assigns a bosonic (fermionic) *superpartner* to every fermion (boson) in the SM, and predicts that the lightest superfermion (sfermion) masses are close to that of their SM partners. The large top quark mass usually plays a central EWSB role here as well. Direct searches at LEP and Tevatron have set lower limits on the masses of various SUSY particles (16). All of these are well above m_b , but there is still enough room for SUSY decays of the top quark. A number of other theories postulate exotic particles and interactions or new space-time dimensions for different reasons, often cosmological. In many of these, the large mass of the top quark makes it a likely connection to new physics.

1.2 The Experimental arena

1.2.1 Producing top

The only facilities where particles as massive as the top quark can be produced at reasonable rates and studied effectively are symmetric high-energy particle colliders, i.e. where the center-of-mass frame coincides with the laboratory frame. To date, only the 1.8 TeV incarnation of the Tevatron had sufficient energy to produce top quarks. The data collected during its Run 1 amounted to ~ 600 $t\bar{t}$ pair events in each of the detector experiments CDF and DØ. Only a small fraction of these passed the stringent selection criteria imposed at the trigger level to suppress enormous QCD backgrounds. This was sufficient, however, to claim discovery of top and make some initial measurements of its properties, principally mass. The current Run 2, with upgraded accelerator and detectors, will result

in perhaps a 100-fold increase in $t\bar{t}$ event yield by 2008. This will allow a more detailed examination of top, sufficient to confirm its SM character, by drastically improving the Run 1 measurements and making possible new ones.

Scheduled to start data collection in 2007, the 14 TeV pp Large Hadron Collider (LHC) is expected to deliver nearly eight million top pair events to each of its two experiments, ATLAS and CMS, in the first year alone. The rate will increase by up to a factor of 10 in subsequent years. Even with a modest rate of acceptance, many rare processes involving the top quark will become accessible.

Beyond the LHC, the most likely next collider would be a 500-1000 GeV e^+e^- linear collider. While the $t\bar{t}$ cross section would be tiny compared to that at the LHC or even Tevatron, the integrated luminosity would be large enough to produce at least half a million top pair events in about five years of running. Moreover, there are two main advantages to such a machine for precision studies. First, $t\bar{t}$ production is an EW process. Theoretical calculations are known to much higher precision in this case, and the absence of enormous QCD backgrounds in experiment would yield extremely high purity samples and nearly fully efficient event collection. Second, because the center-of-mass energy of the colliding beams is exactly known, top quarks could be reconstructed much more precisely. Variable tuning of the beam energy would allow for production threshold scans, giving access to super-precision measurements of mass and width. Control over beam polarization would provide exceptionally detailed couplings determinations. In short, a LC would be an ideal machine for precision top quark physics. However, the main focus here is on recent or approved experiments, i.e., the hadron colliders Tevatron and LHC. We expect a future Annual Review article to concentrate on LC top physics once such a facility is approved. Table 1 summarizes some key

parameters for the colliders mentioned above.

1.2.2 Detecting top

A top quark's production and decay vertices are separated by $\mathcal{O}(10^{-16})$ m, which exceeds the spatial resolution of any detector by many orders of magnitude. Detection of a top quark therefore proceeds through identification and reconstruction of its daughter particles. Fortunately, the large top mass dictates it is not produced highly relativistically. Consequently, its much lighter decay products have good angular separations and high momenta in the laboratory frame. Most end up in the central region of the detector, with \vec{p}_T , the momentum component perpendicular to the beamline exceeding 20 GeV in magnitude ¹.

Top decay products span the entire spectrum of quarks and leptons. Within the SM, the top quark decays almost exclusively into Wb . The W decays almost instantaneously (lifetime $\sim 3 \times 10^{-25}$ s) either *leptonically* into a lepton-neutrino pair: $B(W \rightarrow \ell\bar{\nu}_\ell) = \frac{1}{3}$, ($\ell = e, \mu, \tau$ with equal probabilities) or *hadronically* into a quark-antiquark pair: $B(W \rightarrow q_1\bar{q}_2) = \frac{2}{3}$, ($q_1(q_2) = u(d), c(s)$ with equal probabilities). Hadronic final states manifest themselves as a shower of particles, called a *jet*. If the W decays leptonically, then the charged lepton can be identified with relative ease, τ being an exception, while neutrinos escape direct detection. A graphical representation of the various SM branching fractions of top pairs is shown in Fig. 2. Normally in the experimental context of hadron colliders, only e, μ are referred to as *leptons*, since τ final states behave so differently.

This large and complex set of final state permutations has significant implica-

¹Transverse momentum, \vec{p}_T , implies momentum measurement with a magnetized tracker (e.g. for electrons and muons) while transverse energy, \vec{E}_T , implies calorimeter energy measurement (e.g. for jets). The two have the same physical interpretation, but different resolutions.

tions for data collection. Although a multilayered hardware and software triggering system is carefully designed to retain as many of the most interesting events as possible, and the detector is almost hermetic, some fraction of top events will be lost depending on the decay mode and distribution, as well as the priorities of the experimental program. A brief account of the major issues for particles entering the detector is in order:

- Electrons are recognized with about 90% efficiency by their short interaction length leading to a compact shower in the calorimeter and an associated track of matching momentum in the central tracking volume of the detector.
- Muons are highly penetrating particles that are distinguished by their minimum-ionizing trail all the way through being the only particles to reach the outermost detector layers, with about 90% efficiency.
- Neutrinos escape direct detection because of their tiny weak interaction. Since the beam-axis component of net event momentum varies over a wide range at a hadron collider, only the transverse component of invisible particles' total momenta, \cancel{p}_T (\cancel{E}_T), can be inferred in any given event. Simplistically, it is the negative vector sum of observed particles' transverse momenta. The \cancel{E}_T resolution depends strongly on the content and topology of an event.
- Detection of b quarks is particularly important in selection of top event candidates since most QCD events don't contain them, so their identification reduces backgrounds considerably. A b immediately hadronizes, but typically travels about half a millimeter from the primary interaction vertex before decaying into a jet containing multiple charged particles. Such a displaced decay vertex can be isolated using a good vertex detector by

extrapolating the tracks associated with the jet to a common origin (*secondary vertex tagging*). Jets initiated by gluons and lighter quarks (except sometimes c) are rarely associated with a secondary vertex. Additionally, about 20% of the time a b jet contains a lepton which typically has a lower momentum than a prompt lepton from a W decay. This offers an alternative means for tagging a b quark jet (*soft lepton tagging*). Overall, b quarks can be identified about 60% of the time.

- Tau leptons decay leptonically 36% of the time and hadronically 64%. The leptonic decays result (in addition to two neutrinos) in an electron or a muon that are typically softer than those from W decays. Apart from a very small impact parameter that is difficult to measure, $W \rightarrow \tau \bar{\nu}_\tau \rightarrow \ell \bar{\nu}_\ell \nu_\tau \bar{\nu}_\tau$ ($\ell = e, \mu$) decays cannot really be singled out from $W \rightarrow \ell \bar{\nu}_\ell$ in top events, and are automatically accounted for in the measurements with electron and muon final states. The hadronic modes need special consideration: $\sim 76\%$ of these yield a single charged daughter (*1-prong*) and $\sim 24\%$ yield 3 (*3-prong*). Good pattern-recognition algorithms can exploit the low charge multiplicity and characteristic features of the associated narrow shower in the calorimeter to separate hadronic τ decays from the copious QCD background. The associated neutrino carries away a significant fraction of the τ momentum, making its estimation dependent on the distribution of other objects in the event. Overall, the identification efficiency of hadronic tau decays is about 50%.
- Jets initiated by gluons and lighter quarks have nearly full detection efficiency, although establishing their partonic identity on an event-by-event basis is not possible as they hadronize into overlapping states. Subtle dif-

ferences in profiles of gluon and quark jets may be discernible on a statistical basis. If so, it would be very useful to top quark studies since all jets from top decays are quark initiated (discounting final-state radiation), while jets in the QCD background are predominantly gluon-initiated. This possibility requires further studies in the context of hadron colliders. Jets arising from gluons and lighter quarks will be misidentified as a $b(\tau)$ at a rate of only about 1/200. They fake an electron or muon even more rarely, at about the 1/2000 level.

Top quark decays are no less varied in scenarios beyond the SM. Therefore, identification of all of these *objects* as well as accurate and precise measurement of their momenta are key to studies of the top quark. Detailed description of the detector design and performance specifications are available elsewhere(19,20,21).

Detailed comparisons of the experimental measurements of the nature of top quark production (cross section and kinematics), decay (partial widths, angular correlations among decay products, and so on), and other properties (mass, discrete quantum numbers, etc.), with those theoretically predicted are important probes for new physics. It is a challenge for theorists and experimentalists alike to perform calculations and measurements at the highest possible level of precision. For readers interested in greater detail, especially from an experimenter's point of view, we strongly recommend two excellent articles: Refs. (22) for top quark physics at the Tevatron, and Ref. (18) for that at the LHC. Earlier accounts of the discovery of the top quark can be found in Refs. (23,24).

2 Top Quark Production

At hadron colliders two distinct SM production mechanisms are possible: dominant $t\bar{t}$ pair production, via the strong interaction; and single-top production via the electroweak (EW) interaction. As we shall see, detailed comparison between experimental measurements of physical observables related to top quark production, and SM predictions, is an important probe for new physics.

2.1 Pair production

In the SM, $t\bar{t}$ pairs are produced via quark-antiquark ($q\bar{q}$) annihilation and gluon fusion. Figure 3 shows the corresponding leading order (LO) Feynman diagrams.

The total tree level (Born approximation) $t\bar{t}$ cross section at hadron colliders is a convolution of the parton distribution functions (PDFs) for the incoming (anti)protons and the cross section for the partonic processes $q\bar{q}, gg \rightarrow t\bar{t}$:

$$\sigma(s, m_t^2) = \sum_{i,j} \int_0^1 dx_1 \int_0^1 dx_2 f_i(x_i, \mu_f^2) f_j(x_j, \mu_f^2) \hat{\sigma}_{ij}(\hat{s}, m_t, \alpha_s(\mu_r^2)), \quad (1)$$

where i, j are the possible combinations of incoming gluon or quark-antiquark pairs and $f(x, \mu_f^2)$ are the PDFs, evaluated at some factorization scale μ_f corresponding to a scale in the problem, such as m_t , and a value x which is the fraction of incoming (anti)proton energy that the parton carries. The partonic subprocess cross sections, integrated over phase space, are functions of the center-of-mass energy $\sqrt{\hat{s}}$, the top quark mass m_t , and the QCD strong coupling constant α_s evaluated at a renormalization scale μ_r , also typically taken to be one relevant to the process, e.g. m_t , but it does not have to be the same as μ_f . At higher orders, the partonic cross section also depends on μ_f, μ_r : $\hat{\sigma}_{ij}(\hat{s}, m_t, \mu_f, \mu_r, \alpha_s(\mu_r^2))$.

At the Tevatron, $t\bar{t}$ production occurs close to, but not quite at threshold. The

maximum of $d\sigma_{t\bar{t}}/d\hat{s}$ occurs around $3/2$ the threshold value, and the average speed of the top quarks is about $\beta \approx 0.5$. If for threshold we set $x_i \approx x_j = x_{\text{thr}}$, from $\hat{s} = x_i x_j s$ we obtain $x_{\text{thr}} \approx \frac{2m_t}{\sqrt{s}}$. In Tevatron Run 1, $x_{\text{thr}} \approx 0.2$, where the quark distribution functions are considerably larger than that for the gluon, $q\bar{q}(gg) \rightarrow t\bar{t}$ accounted for 90%(10%) of the cross section ². In Run 2, $\sqrt{s} = 2.0$ TeV, the total cross section is about 40% larger, with 85%(15%) coming from an initial $q\bar{q}(gg)$ pair. At the LHC the situation is reversed: $x_{\text{thr}} \sim 0.025$, a regime where gluons dominate, so the $q\bar{q}(gg)$ contributions are about 10%(90%). Table 1 summarizes the $t\bar{t}$ cross sections at the Tevatron, LHC and a LC, compared to other important SM processes. At the Tevatron, roughly one in 10^{10} collisions produces top quark pairs. In Run 1 the average production rate was $\sim 5 \cdot 10^{-5}$ Hz, expected to reach $\sim 7 \cdot 10^{-4}$ Hz in Run 2. In comparison, the rate will be about 10 Hz at the LHC, a true “top factory”.

The uncertainty in $\sigma_{t\bar{t}}^{LO}$ at hadron colliders is large, $\sim 50\%$. The primary source centers around the scale choices μ_f and μ_r , and their effects on α_s . Furthermore, α_s is relatively large, so additional terms in the perturbative expansion for the cross section can be significant. These issues can be addressed by calculating the cross section at next-to-leading order (NLO) in perturbation theory, which we discuss in the next section. Additional, smaller sources of uncertainty are the PDFs and the precise values of m_t and $\alpha_s(M_Z^2)$. At the Tevatron the cross section sensitivity due to PDFs is small mainly because the process is driven by the well measured quark distributions. This is not the case at the LHC, where a $\sim 10\%$ uncertainty in $\sigma_{t\bar{t}}$ comes from the PDF for the dominant gg component.

²For the partonic cross sections, $\sigma_{gg} > \sigma_{q\bar{q}}$, but parton densities are the dominant effect.

2.1.1 Higher order corrections and theoretical uncertainties

At LO the $t\bar{t}$ cross section is usually evaluated for $\mu_f = \mu_r = m_t$, as m_t is the only relevant scale in the problem (one could also argue for $2m_t$ for α_s , but $\mu_r = \mu_f$ is the more common choice). Since this is much larger than the scale of QCD confinement, $\Lambda_{QCD} \sim 200$ MeV, the calculation can be trusted to behave perturbatively. But what does the scale choice signify? After all, both PDFs and $\alpha_s(M_Z^2)$ are data extracted from experimentally measured cross sections. However, they are based on processes very different from those we wish to consider at hadron colliders. We have to let α_s *run* and the PDFs *evolve* from the scales relevant in extraction to the scales relevant for application. The calculation of the process under consideration is separated into two parts: the perturbative hard scattering (here, $q\bar{q}, gg \rightarrow t\bar{t}$), and the perturbatively resummed PDF evolution which uses non-perturbative input. To this end, the scales μ_r, μ_f are introduced to separate the perturbative and non-perturbative parts of the calculation.

By construction, physical observables in a renormalizable field theory do not depend on a scale. But this is true only to all orders in perturbation theory, which is impossible to calculate. At fixed order, the scale independence is not realized. Higher orders help restore this, removing bit by bit the scale dependence we artificially introduced. Varying the scale at a given order gives one an idea of the residual calculational uncertainty.

In a higher-order calculation, all diagrams that contain the same order in the relevant coupling must be included. Here, this is α_s . Thus, the full $\mathcal{O}(\alpha_s^3)$ NLO calculation (25) includes both real parton emission and virtual (loop diagram) corrections, even though the different parts do not contain the same number or even type of final state particles. The NLO corrections increase $\sigma_{t\bar{t}}$ by about

30%, with the uncertainty from varying the scale choice reduced to about 12%.

An important point to note is that the order of the hard scattering process evaluated must match that of the PDF set used. At each higher order in α_s , there are strong cancellations between terms in the PDF evolution and in the hard scattering real emission, which come from the artificial dependence on μ_f introduced by factorizing the problem in the first place. For NLO calculations, NLO PDFs must be used; for LO calculations such as parton shower Monte Carlo (MC), LO PDFs must be used. Noncompliance can introduce large errors.

The NLO calculation of $\sigma_{t\bar{t}}$ experiences large logarithms $\sim \alpha_s \log^2 \beta$, where β is some definition of the threshold dependence (which can vary at NLO), arising from real emission of a soft gluon. As $\beta \rightarrow 0$ at threshold, the calculation becomes unstable. Fortunately, real radiation there is restricted by phase space, so soft gluons approximately *exponentiate*: an $(\alpha_s \log^2 \beta)^n$ term appears at all orders in perturbation theory, with a coefficient at each order of $\frac{1}{n!}$ from permutations over identical gluons, resulting in a series that is simply an exponential containing $\alpha_s \log \beta$. Calculating it is called *resumming* the large logs. This behavior is a direct consequence of soft gluon emission in QCD factorizing both in the matrix element and in phase space. A leading-log (LL) resummation takes care of the $(\alpha_s \log^2 \beta)^n$ series, a next-to-leading-log (NLL) resummation the $(\alpha_s (\alpha_s \log^2 \beta))^n$ series, and so on. This is an overly simplistic picture, but gives one an idea of what resummation calculations address.

According to one recent NLO+NLL complete resummation calculation (26), with PDF-updated results for the LHC in Sec. 2 of Ref. (18), resummation effects are at the $\mathcal{O}(5\%)$ level for both the Tevatron and LHC. Results are $\sigma_{t\bar{t}} = 5.06(6.97)$ pb for $p\bar{p}$ collisions at $\sqrt{s} = 1.8(2.0)$ TeV and 825 pb for pp

collisions at 14 TeV, where the uncertainties are from scale variation. Another $\sim 6\%$ contribution comes from PDFs and α_s .

Another recent Tevatron-only study (27) is a partial NNLO+NNLL calculation, where they expand the exponential expression to the first three powers of the large logs at $\mathcal{O}(\alpha_s)$ and $\mathcal{O}(\alpha_s^2)$. This study finds a 5 – 20% uncertainty depending on the $t\bar{t}$ kinematics considered, and averages the results to construct total estimates of $\sigma_{t\bar{t}}(1.8\text{TeV}) = 5.8 \pm 0.4 \pm 0.1$ pb and $\sigma_{t\bar{t}}(2.0\text{TeV}) = 8.0 \pm 0.6 \pm 0.1$ pb, where the first uncertainty is due to kinematics and the second is from scale uncertainty.

The Tevatron results of Refs. (26, 27) are not necessarily contradictory, since they use different methods that selectively incorporate different higher-order terms. For uncertainties at the LHC, the relation is (18) $\frac{\delta\sigma}{\sigma} \sim 5\frac{\delta m_t}{m_t}$, i.e., if 1 GeV in δm_t is achievable, then the cross section should be known to about 3% experimentally. This makes improvements in $\sigma_{t\bar{t}}^{NLO}$ desirable, although a complete NNLO calculation is not likely to be completed soon. At the very least, it would be useful to have an improved understanding of PDFs, such as a more sophisticated PDF-uncertainty analysis.

Besides the soft gluon effects, Coulomb effects may enhance or deplete the cross section near threshold. However, these are found to be negligibly small for $t\bar{t}$ production at both the Tevatron and LHC (28), much smaller than the inherent uncertainty in the NLO+NLL calculations. The same holds true for EW corrections, found to be -0.97% to -1.74% of $\sigma_{t\bar{t}}^{LO}$ for $60 < M_H < 1000$ GeV (29).

2.1.2 Experimental measurements: cross-sections, kinematics

We now turn to the question of how to measure experimentally the $t\bar{t}$ production cross section and how accurate these measurements are expected to be.

Within the SM, the top quark decays almost exclusively into a W boson and a b quark. The channels and branching fractions for $t\bar{t}$ decays can be readily derived from those for W decays given in Sec. 1.2.2. Because of the uniqueness of their experimental detection, channels involving τ leptons are usually treated separately. In the context of object identification in the detector, unless noted otherwise, a “lepton” normally refers to e or μ . Thus, the $t\bar{t}$ final state is categorized as “dilepton” (branching fraction = 5%), “single-lepton (plus jets)” (30%) and “all-hadronic” (44%) depending on whether both, only one, or neither of the two W bosons decay leptonically into an electron or a muon and the corresponding neutrino (Fig. 4). The remaining 21% involves τ leptons: 6% for “ τ -dilepton” ($e\tau$, $\mu\tau$, $\tau\tau$) and 15% for τ +jets.

- **Modeling $t\bar{t}$ production**

Accurate simulation of collision events is critical to the understanding of how to derive reliable physics measurements from the detector data. Experimentalists use MC generators such as PYTHIA (30), HERWIG (31) or ISAJET (32) to model $t\bar{t}$ production in hadron collisions. These include approximate treatments of higher order perturbative effects (initial and final state gluon radiation), hadronization of the final state partons, underlying event, and secondary particle decays. They begin by using an exact matrix element calculation (QCD or EW) of the hard scattering process, such as $q\bar{q} \rightarrow t\bar{t}$, then simulate the emission of additional partons from the incoming and outgoing partons in the hard process. This is done with a *parton shower* algorithm evolving the emitted parton energies downwards to a cutoff point, where hadronization takes over.

A more detailed description of these MC programs can be found e.g. in Ref. (18). The events these generators produce are then combined with the

simulation of the detectors' response to the final state particles. Event selection *cuts* can then be studied to understand how best to optimize the signal acceptance while reducing backgrounds from other physics processes that can fake a $t\bar{t}$ signature.

There are “small” discrepancies between some of the predictions in these MC programs. For example, PYTHIA and HERWIG differ in the amount of gluon radiation that they introduce (33, 34). Tests comparing distributions from the MC predictions to the NLO calculations can be found e.g. in Ref. (35) which concludes that in the low- p_T region HERWIG more closely approximates the NLO calculations.

It is clear that as larger $t\bar{t}$ datasets are gathered by the experiments, more detailed comparisons between data and MC predictions will be feasible and a positive feedback loop will be established. This will lead to improved understanding of mechanisms behind the more subtle aspects of $t\bar{t}$ production. Accurate modeling will be critical in detecting any possible deviation from the SM predictions.

- **Event selection and backgrounds**

It is important to understand how the rare $t\bar{t}$ events are selected from the flood of other events generated in hadron collisions, and how they are separated from backgrounds that pass the same selection criteria. We discuss the experiments at the Tevatron and then point out the differences, if any, for the LHC.

As would be expected in the decay of a massive, slow-moving particle ($\beta \ll 1$) into almost massless ones, the final state particles in top decay typically carry large transverse momentum in the lab frame ($p_T > 15 - 20$ GeV), and often go

into the more central part of the detector ($|\eta| < \sim 2.5$)³ Therefore, regardless of channel, the first experimental criteria for detecting top events is requiring high p_T for all decay products This requirement goes a long way in suppressing backgrounds, especially processes with jets from QCD radiation, which have an exponentially falling E_T spectrum, and processes in which \cancel{E}_T is an artifact of instrumental imprecision, not the escape of real, high- p_T neutrinos. Other topological cuts, such as requiring that the leptons and \cancel{E}_T are isolated from jet activity and more global event variables such as *scalar* E_T (H_T , the scalar sum of E_T of all observed objects), sphericity and aplanarity⁴ help enhance the signal-to-background ratio ($S : B$). The latter two are variables calculated from the eigenvalues of the normalized momentum tensor. Aplanarity \mathcal{A} , proportional to the smallest of the 3 eigenvalues, measures the relative activity perpendicular to the plane of maximum activity. Sphericity \mathcal{S} , proportional to the sum of the two smaller eigenvalues, measures the relative activity in the plane of minimum activity. Top quark events typically have larger values of H_T , \mathcal{S} , \mathcal{A} . Finally, the b -tagging requirement eliminates most non-top QCD contamination of the signal, about a 100-fold reduction, compared to $\sim 75\%$ of the top events yielding at least one tagged b -jets⁵. Tagging heavy-flavor jets with soft leptons helps disentangle systematic uncertainties of the QCD heavy-flavor content.

Remaining backgrounds in the all-hadronic channel arise mainly from QCD multi-jet production, in which b tags from real heavy-flavor quarks (mostly b , but also some c) or from fakes (gluons or light quarks) are present. The $S : B$ ranges from 1:5 to 1:1 depending on details of the selection. In the single-lepton channel

³ $\eta = \frac{1}{2} \frac{E+p_z}{E-p_z}$ is called the *pseudorapidity*, which for massless particles is $\eta = -\ln\left(\tan\frac{\theta}{2}\right)$.

⁴Defined e.g. in Ref. (36).

⁵The efficiencies of Sec. 1.2.2 have to be moderated by the fiducial acceptance of the detector.

the most copious background is from W +jets events, before b -tagging, and from W +heavy-flavor after. The $S : B$ after b -tagging is typically between 1:1 and 4:1, again depending on the exact criteria. For dileptons, $S : B \approx 1 : 2$, even without b -tagging, with backgrounds coming mainly from WW , $Z \rightarrow \tau^+\tau^-$ and Drell-Yan production, all with additional jets from QCD radiation. The background in this case becomes negligible if the requirement of b -tagging is added. This is because these backgrounds are all either EW suppressed, or arise only from several small branching fractions successively. Including branching fractions and efficiencies of the full chain of selection criteria, only a few percent of the $t\bar{t}$ events produced in the collisions make it to the final sample. In Run 1 an estimated 5% made it to the all-hadronic candidate pool, about 5% to the single-lepton, and only about 1% to the dilepton pool.

An excess of about 10 dilepton events over an expected background of 4 events was observed in the combined data samples of CDF and DØ. Some of these candidates have been suggested as having unusual kinematics (37); Run 2 should resolve this question. In the single-lepton channel, with [without] b -tags, an excess of about 60 [10] events was observed over an expected background of about 40 [9]. In the all-jet channel DØ [CDF] observed an excess of 16 [43] events over a background of about 25 [144].

At the LHC, very pure signals should be obtained in the dilepton and single-lepton channels. For 10 fb^{-1} , with similar selection criteria as those used at the Tevatron, about 60,000 b -tagged dilepton events are expected, with a $S : B \approx 50$ (18). In the single-lepton channel, this will be close to one million b -tagged events. Since the cross section for QCD W +jets grows more slowly with collision energy than does $t\bar{t}$, $S : B \approx 20$ should be possible. However, extracting such

a clean signal on the all-jets channel out of overwhelming QCD background is not deemed feasible. Ongoing studies selecting on more sophisticated kinematical variables and using multivariate discriminants show a paltry $S : B \approx 1 : 6$.

Figure 5 shows the $t\bar{t}$ cross section results individually from CDF and DØ in Run 1 for the different decay channels, and the combined results (2). The measurements, within their $\sim 30\%$ uncertainties (dominated by the statistical component), are consistent with SM predictions. In Run 2, a precision of 10% is believed achievable with only 1 fb^{-1} of data. Many other factors will then limit the measurement, mostly from calculation of the total acceptance (lepton and b -tagging efficiencies, event generator systematics, jet energy scale and luminosity measurement uncertainty, amongst others). Prospects for reducing these various components are addressed as needed in Sec. 4.

2.2 Single top production

Single top quark production cannot occur in flavor-conserving QCD, so it probes the charged-current weak interaction connecting top to the down-type quarks, with amplitudes proportional to the CKM matrix element V_{tq} ($q = d, s, b$). This interaction has a vector minus axial-vector ($V - A$) structure because only the left-chiral component of fermions participate in the $SU(2)$ gauge interaction. Also due to the weak interaction, single top quarks are produced with nearly 100% polarization, which serves as a test of the $V - A$ structure.

Figure 6 shows the three different ways a hadron collision can produce top quarks singly. The process $q\bar{q} \rightarrow t\bar{b}$ via a virtual s -channel W boson probes the top quark with a timelike W boson, $q^2 > (m_t + m_b)^2$, while the W -gluon fusion (t -channel) processes involve a spacelike W boson, $q^2 < 0$. These production

mechanisms are thus complementary, as they probe the charged-current interaction, in different q^2 regions. In the third process, *associated-production*, the W is real and produced in association with the top quark.

The cross sections for all three processes are proportional to $|V_{tb}|^2$. Therefore, measuring the single top quark production cross section provides a direct probe of $|V_{tb}|$ and the weak tbW vertex in general (we discuss V_{tb} in detail in Sec. 4.5). Each process can be affected by new physics in a different way. It is therefore important to observe and study each process separately, to the extent allowed by the overlap of the signatures. Studies show that the s - and t -channels should be observed at the Tevatron in Run 2 with a small data sample of only a few fb^{-1} . The associated production process, however, is smaller in the SM and will be observed only at the LHC. As we shall see, the observation of single top is even more challenging than $t\bar{t}$. Not only are the cross sections smaller, but the final state signatures suffer from larger background due to the less distinctive topology of fewer high- p_T jets, leptons, b-quarks, and \cancel{E}_T .

It is interesting to note that $p\bar{p} \rightarrow t\bar{b} \rightarrow Wb\bar{b}$ is a significant background to the SM Higgs search channel $p\bar{p} \rightarrow W^+H; H \rightarrow b\bar{b}$. Top quarks, produced either singly or in pairs, will generally be a background to a host of other channels of possible new physics. So even if we are satisfied of the SM properties of top, we must strive for exacting precision in modeling top for the sake of searches for new phenomena.

2.2.1 Single top production in the s -channel

The purely EW s -channel single-top process is shown in Fig. 6(a). As this arises from initial-state quarks, where the PDFs are well-known, the hadronic cross

section has relatively small PDF uncertainty. The NLO calculations (39, 40, 41) show that, for both the Tevatron and the LHC, there is only a relatively small residual dependence on the scales μ_f, μ_r , about $\pm 2\%$. Resummation effects are small, of the order of 3% (40) and Yukawa corrections (loops involving the Higgs sector fields) are negligible ($< 1\%$) at both colliders. The cross section does change, however, by about $\mp 10\%$ at both the Tevatron and LHC if m_t is varied by ± 5 GeV. Thus, 1-2 GeV precision in m_t would be desirable to avoid increasing the theoretical uncertainty further. Because the cross section is potentially so precisely known, this channel may provide the best direct measurement of $|V_{tb}|$ at the Tevatron (see Sec. 4.5).

In Run 1, the cross section was predicted to be about 0.70 ± 0.04 pb. This is roughly 8 times smaller than $\sigma_{t\bar{t}}$, and suffers from comparatively larger backgrounds. An increase of only about 30% is expected in Run 2, while an additional factor of 24 is expected for the LHC. Table 2 shows the results of the fully differential NLO calculations (41). In spite of the small cross section, as we discuss below, both CDF and DØ started the search for single top already during Run 1, both to establish the technique that will bear fruit in Run 2, and on the chance that new physics increases this cross section greatly beyond SM expectations.

2.2.2 Single-top production in the t -channel

The W -gluon fusion cross section is illustrated by the Feynman diagrams in Fig. 6(b,c). These diagrams are closely related: diagram (b) shows the hard matrix element to calculate when the initial parton is treated with a b quark density (b in the proton sea arises from splitting of virtual gluons into nearly collinear $b\bar{b}$ pairs); diagram (c) is relevant if the initial parton is treated as a gluon, and

the extra final-state b quark is typically required to appear at large (experimentally observable) p_T . Calculation is less precise than for the s -channel because it involves gluon or b quark PDFs, which have relatively large uncertainties. In general the inclusive cross section with resummed logarithms predicts the total single top rate more precisely. On the other hand, an exclusive calculation using gluon densities and a finite transverse momentum ‘incoming’ bottom might in some cases give better kinematic distributions. Recent literature (42) has highlighted this and corrected some improper uses of b parton densities, in the context of Higgs boson production. There, some factorization scale issues have been shown to be important, which eventually must be applied to the single top case.

The final state in this channel is Wbq , with an occasional additional \bar{b} antiquark: $\sim 75\%$ of the total cross section occurs for $p_T(\bar{b}) < 20$ GeV (43), too low to be observed. Absence of the additional b -jet helps differentiate this process from the s -channel, but the primary distinction is the additional light quark jet. This will typically be emitted at large rapidity, very forward in the detector, where most hard QCD events do not emit jets. This is sometimes known as a *forward tagged jet*.

This channel benefits from a larger production rate compared to the s -channel. At the Tevatron it is about a factor of three larger, while at the LHC it is about a factor of 23. The NLO cross section (44,45,46) retains a somewhat larger scale dependence than in the s -channel case, about 5% at both the Tevatron and the LHC, but this is still quite good. If the top mass is changed by ± 5 GeV, the cross section changes by about $\mp 8\%$ ($\mp 3\%$) at the Tevatron (LHC), so its dependence on m_t is comparatively smaller and likely not the limiting factor in theoretical uncertainty. The Yukawa corrections are also small, $\approx 1\%$. The fully differential

NLO cross sections for the Tevatron and LHC are listed in Table 2 (41).

2.2.3 Associated production channel

Associated production of single top, tW , shown in Figs. 6(d,e), proceeds via an initial gb pair, which makes the cross section negligible at the Tevatron. However, at the LHC it contributes about 20% of the total single top cross section. Like the t -channel case, one of the initial partons is a b quark. However, unlike the t -channel, the rate of this process scales like $1/s$. This, combined with the higher x values needed to produce a top and a W and correspondingly scarcer quark parton densities, leads to a cross section about five times smaller than that of the t -channel, despite the fact that associated production is order $\alpha_s\alpha_W$ rather than α_W^2 (the ratio of strengths is $\frac{\alpha_s}{\alpha_W} \approx 10$). This cross section has been calculated only at LO, with a subset of the NLO calculations included (47); its relative unimportance make a full NLO calculation not likely necessary. Cross section uncertainty is $\approx 10\%$ from PDFs and $\approx 15\%$ from scale variations. The cross section at the LHC in the SM is 62 pb with a total uncertainty of $\sim 30\%$ (see also Table 2).

2.2.4 Experimental status and prospects

Combining the s - and t -channel cross sections, the total single-top production rate is about 40% of $\sigma_{t\bar{t}}$ at both Tevatron and LHC. Observing singly produced top quarks is more difficult than those pair-produced, because the final state of single-top events is not as rich in particle content or pole structure. Experimental searches for single top have to take into account subtle kinematical differences between the relatively larger backgrounds and the various single-top production

channels. In all cases, at least one W boson and one b jet are present in the final state. To suppress backgrounds from QCD, one is forced to focus on the leptonic W decay sub-channels, just as the all-hadronic $t\bar{t}$ channel is difficult at the Tevatron and an extreme proposition at the LHC; and of course b -tagged events. Therefore, the starting sample for these searches requires a single high- p_T isolated lepton, large \cancel{E}_T and a b -tagged jet. The challenge is to understand very precisely the rate and kinematics of all processes that contribute to the “ $W + b$ +jets sample”. Only at that point, and with enough data that a statistically significant signal can be extracted, can a credible claim of single-top observation be made. We now briefly discuss the searches made at the Tevatron in Run 1 and the prospects for Run 2 and the LHC.

Run 1 searches:

The CDF and DØ experiments have searched for each of the potentially accessible s - and t -channel signatures separately, and CDF has also performed a combined search, which looked for single top in the W +jets sample, with the W decaying leptonically into e or μ , and allowing up to 3 jets. The invariant mass of the lepton, \cancel{E}_T and highest- p_T jet must lie between 140 and 210 GeV, bracketing the top mass. This was followed by a likelihood fit to H_T , the scalar p_T sum of all final state objects seen in the detector. This distribution is on average softer for non-top QCD backgrounds and harder for $t\bar{t}$ production, with single top falling somewhere between. The limit extracted by this technique is $\sigma(p\bar{p} \rightarrow t + X) < 14$ pb at 95% C.L. (11).

For the search that separates s - from t -channel production, CDF took advantage of b -tagging using displaced vertices, and of the fact that usually only one b -tagged jet can be expected in the t -channel case. This is because the \bar{b}

tends to be collinear with the initial gluon, therefore having too-low p_T to be observed. The single and double-tagged events in the $W+2$ -jet samples were reconstructed separately and subjected to a likelihood fit. The resulting limits (11) are $\sigma_{s\text{-chan}} < 18$ pb and $\sigma_{t\text{-chan}} < 13$ pb.

The $D\bar{O}$ experiment used a neural network trained differently for the different channels, and considered tagged and untagged events (tagging for $D\bar{O}$ was done by associating non-isolated soft muons to semileptonic b -decays). The limits obtained are (12): $\sigma_{s\text{-chan}} < 17$ pb and $\sigma_{t\text{-chan}} < 22$ pb. These limits are about an order of magnitude above the expected SM values (see Table 2), but still useful as an establishment of technique, and to rule out major deviations due to new physics.

The backgrounds in these searches arose mainly from W +jets, QCD multijets and $t\bar{t}$, with a $S:B$ ratio in the range of 1:10 to 1:25, depending on channel and the strictness of event selection. It proved crucial to use b -tagging to reduce the background from QCD multijets (only fakes remained) and from W +jets (principally only W +heavy-flavor remained).

Run 2 and LHC plans:

At Tevatron Run 2 and the LHC, emphasis will be on the slight differences in kinematic distributions between the various signal and background processes to extract the signal in each of the three channels. Useful variables include jet multiplicity, event invariant mass, reconstructed top invariant mass, invariant mass of all jets, E_T of the jets (including forward jets), H_T , and others. Sophisticated pattern-recognition techniques, such as neural networks with these or similar inputs, will play a large role. Such techniques are now being perfected in order to conduct these searches with better precision.

Run 2 with only 2 fb^{-1} should be able to achieve 20 – 30% accuracy for the s - and t -channel cross section. At the LHC, the t -channel, the highest yield of the three, is expected to give the most precise cross section and thus $|V_{tb}|$ measurement. A $S:B$ of about 2:3 should be reached, with statistical uncertainty of 1 – 2%. For the s -channel at LHC, requiring 2 high- p_T b -tagged jets and no other jets in the event yields $S:B \approx 1:12$ and statistical uncertainty of about 6%. For the associated production channel (accessible only at LHC) to maximize signal significance, hadronic decays of the W may be included in the search by constraining a two-jet invariant mass to be close to M_W . This requirement, together with the higher jet multiplicity in the event, helps reduce backgrounds. Simulations predict $S:B \approx 1:4$ and statistical uncertainty of about 4%.

It is not easy to estimate firmly the systematic uncertainties in these measurements. Luminosity alone can contribute at the level of 5% or more. Further work on this issue must build on the experience gained at the Tevatron.

2.3 Sensitivity to New Physics

Top quark production at hadron colliders, be it $t\bar{t}$ or single top, is an ideal place to look for new physics. If there is any new physics associated with the generation of mass, it may be more apparent in the top quark sector than with any of the other lighter, known, fermions. Many models predict new particles or interactions that couple preferentially to the third generation and in particular to the top quark. These models extend the strong, hypercharge or weak interactions in such a way that the new groups spontaneously break into their SM subgroup at some scale: $SU(3)_h \times SU(3)_l \rightarrow SU(3)_C$, $SU(2)_h \times SU(2)_l \rightarrow SU(2)_W$, and $U(1)_h \times U(1)_l \rightarrow U(1)_Y$, where h represents the third (heavy) generation and l the

first two (light) generations. As a result, one would expect production rate and kinematic distributions of the decay products to differ from the SM predictions.

Here we highlight only a few scenarios, simply to illustrate the rich ways top production can be affected by physics beyond the SM. Along the way we refer the reader to key papers in the vast literature on this subject.

Top pair production:

In $t\bar{t}$ production, it is especially interesting to study the invariant mass distribution of the top pair, $d\sigma/dm_{t\bar{t}}$, since it can reveal resonant production mechanisms. Other interesting kinematical distributions are the angle of the top quark with respect to the proton direction (Tevatron only) in the center-of-mass system (48), and the top quark and W boson p_T spectra. A partial list of new phenomena that can contribute to the cross section enhancements and to the distortion of the SM kinematical distributions can be found in Refs. (49, 50, 51, 52, 53, 54, 55, 48).

One potential source of new physics in $t\bar{t}$ production is SUSY correction to QCD (38), SUSY being one of the leading candidates for new physics. The conclusion is that aside from special regions in MSSM parameter space, the contribution is at most a few percent correction to the total $t\bar{t}$ rate or the $m_{t\bar{t}}$ spectrum, making it very difficult to detect SUSY this way.

In another scenario, if the top is a composite quark then there would be effects modifying the cross section, depending on the properties of the constituents of the top quark. If these carry color, scattering proceeds through gluon exchange (56, 57). If the light quarks are also composite then $q\bar{q} \rightarrow t\bar{t}$ can proceed directly through the underlying composite interactions, as well as by QCD gluon exchange (58). In either case, compositeness would result in an enhancement of the $t\bar{t}$ cross section over the SM value which could manifest itself as an enhance-

ment in $d\sigma/dm_{t\bar{t}}$ at large $m_{t\bar{t}}$.

Many theories postulate heavy resonances decaying to $t\bar{t}$, such as technimesons in technicolor models (49, 59) (e.g. $gg \rightarrow \eta_T \rightarrow t\bar{t}$) or other models of strong EWSB (50, 52). Variants of technicolor theories, such as topcolor (60, 61) and topcolor-assisted technicolor (TC2) (61), hypothesize new interactions, e.g. mediated by top-gluons or new weak bosons that are specifically associated with the top quark, that give rise to heavy states: $q\bar{q} \rightarrow g_t \rightarrow t\bar{t}$, $q\bar{q} \rightarrow Z' \rightarrow t\bar{t}$, etc. Since $t\bar{t}$ production at the LHC is dominated by gg fusion, color octet resonances (*colorons*) could also be produced (62). More recently, extra-dimensional theories propose scenarios in which new scalar bosons have couplings preferential to the third generation. Some scenarios in which only these bosons live in the extra dimensions predict particles very similar to the topcolor Z' (55).

Top quark pair production can be thought of as the modern day Drell-Yan, probing the ultra-heavy intermediate states predicted by various models. Present and future experiments should patiently scan the $m_{t\bar{t}}$ spectrum for surprises. CDF and DØ have already in Run 1 searched for narrow vector resonances in $m_{t\bar{t}}$ in the single lepton channel. Within the limited statistics of these samples (63 events, with $S : B \approx 1:1$ for CDF), no significant peaks were observed. Even though the searches were in principle model-independent, limits on specific models can be extracted. CDF finds that the existence of a leptophobic Z' in a TC2 model with mass < 480 GeV (< 780 GeV) can be excluded at 95% C.L. if its width is 1.2%(4%) of its mass (63). The DØ search excludes $M_{Z'} < 560$ GeV at 95% C.L. for $\Gamma_{Z'} = 0.012M_{Z'}$ (64). These searches will continue in Run 2, extending limits considerably, or perhaps revealing something more interesting.

Many other kinematical distributions in the top samples were examined in

Run 1 (65, 22), testing consistency with SM expectations (see e.g. Refs. (35, 34, 48)). Within the limited statistics of the samples, no significant deviations from the SM have yet been observed. Nonetheless, some intriguing features, such as large \cancel{E}_T and lepton p_T , have been noticed in the dilepton samples (37). These could conceivably be attributed to SUSY production. However, multi-variable consistency checks do not show overall significant deviations (66). Other samples that overlap with top, such as the CDF b -tagged W +jets sample, show very interesting features, with certain sub-samples containing soft-lepton tags showing minor deviations from SM expectations. Run 2 data will help decide if these are statistical fluctuations or if some new physics is hiding in the data.

The LHC could, of course, discover particles with masses larger than those accessible at the Tevatron. Studies for the ATLAS experiment show 5σ discovery potential curves for $(\sigma \cdot \mathcal{B})$ v. $m_{t\bar{t}}$ for a hypothetical narrow resonance (18). Particles as massive as 2 TeV could be discovered with datasets of 300 fb^{-1} if $\sigma \cdot \mathcal{B} > 50 \text{ fb}$.

Single top production:

New physics could also be discerned in single-top production by introducing new weak interactions (67, 68, 69, 46, 70); via loop effects (71, 62, 72, 73, 74); or by providing new sources of single-top quark events (46, 62, 75, 76, 77).

Resonances can also appear in single-top production. For example, a new heavy vector boson W'^{\pm} or charged scalar ϕ^{\pm} , new $SU(2)$ structure or extra-dimensions, can all contribute additional diagrams analogous to those in Fig. 6 and affect the rates and kinematics differently. The s-channel process would be particularly sensitive to these states, but the t - and associated production channels are not expected to be affected significantly (46). Charged scalars feature in models with

more than one Higgs doublet, such as the MSSM, and in topcolor. Processes such as $c\bar{b} \rightarrow \pi_t^+ \rightarrow t\bar{b}$ contribute significantly to the s -channel rate (a factor of two enhancement is possible at the Tevatron and even more at the LHC). On the other hand, non-SM flavor-changing neutral currents (e.g. a Ztc vertex) would be difficult to see in the s -channel, while the t -channel would exhibit large effects (46).

Regardless of the specific search for new physics in top quark production, an important point is that one has to be careful, when studying kinematical distributions, in making event selections optimized to detect pure SM production that may dilute the effects of new physics. For example, a resonance in $t\bar{t}$ production may distort the summed E_T and sphericity or aplanarity distributions of candidate events from their SM expectation (48).

3 Top Quark Decays

The SM predicts $\mathcal{B}(t \rightarrow bW) > 0.998$. Other decays allowed in the SM are not only rare, but also mostly too difficult to disentangle from backgrounds to be observed in the foreseeable future. Nevertheless, one must try to be sensitive to all conceivable signatures of top quark decay, as some can be enhanced by several orders of magnitude in scenarios beyond the SM, falling within the LHC's reach. We first review the SM decays, then discuss possibilities in the presence of new physics.

3.1 Standard Model top quark decays

After $t \rightarrow bW$ ⁶, the next most likely modes are the off-diagonal CKM decays $t \rightarrow Ws, Wd$. Together with $t \rightarrow WbZ$, these are the only ones allowed in the SM at tree level and discussed in Sec. 3.1.1⁷. Flavor-changing neutral currents (FCNC) decays, $t \rightarrow X^0 q$, where $X^0 = g, \gamma, Z, H$ and $q = c, u$, are loop induced and highly suppressed by the GIM mechanism (78). Branching fractions are typically $\mathcal{O}(10^{-13})$. We discuss these in Sec. 3.1.2.

3.1.1 Charged current decays

In the SM, $t \rightarrow Wb$ is described purely by the universal $V - A$ charged-current interaction. Being on-shell, however, the W boson's helicity in top decays is very different from that in the decays of any other quark, where the W is highly virtual. The amplitude for positive helicity W^+ boson is suppressed by a chiral factor $\frac{m_b^2}{M_W^2}$, so the W helicity is a superposition of just the zero and negative helicity states. At tree level in the SM, the fraction \mathcal{F}_0 of the longitudinal (zero helicity) W bosons in the top rest frame is (79, 80):

$$\mathcal{F}_0 = \frac{m_t^2/M_W^2}{1 + m_t^2/M_W^2} = 0.701 \pm 0.016 \quad (2)$$

for $m_t \gg M_W$. The large top mass exposes the longitudinal mode of the W , so precise measurement of \mathcal{F}_0 serves as a stringent test of the SM. To this end, CDF analyzed the lepton p_T spectrum in $t\bar{t}$ single lepton final states in Tevatron Run

⁶Henceforth, we won't distinguish flavor or antiflavor whenever the symmetry is obvious. All statements are equally valid under charge conjugation.

⁷The radiative decays $t \rightarrow Wbg$ and $t \rightarrow Wb\gamma$ are common, but do not offer any fundamental new insight unless the branching fractions turn out to be significantly different from the SM predictions (0.3 and 3.5×10^{-3} respectively, for $E_{g/\gamma} > 10$ GeV at LHC). These channels are generally treated inclusively with $t \rightarrow Wb$.

1. Assuming a pure $V - A$ coupling, they obtained $\mathcal{F}_0 = 0.91 \pm 0.37(\text{stat.}) \pm 0.13(\text{syst.})$, consistent with the SM (16, 81). The statistical uncertainty will be reduced by an order of magnitude in Run 2, and to a negligible level at the LHC. Improvement in the systematic uncertainty has yet to be estimated, but should be better than a factor of 2.

Variables like the angle between the lepton and its parent W direction in the top rest frame depend on the W helicity. Such variables as $M_{\ell b}$ can therefore be used to estimate the relative W helicity fractions, and thus the $V + A$ component in top decay. CDF's Run 1 analysis gives $f(V + A) = -0.21_{-0.25}^{+0.42}(\text{stat.}) \pm 0.21(\text{syst.})$ (preliminary) (82).

The ‘‘radiative’’ decay $t \rightarrow WbZ$ has been suggested (83) as a sensitive probe of the top quark mass, since the measured value of m_t makes this decay close to threshold. The branching fraction varies by a factor of ~ 3 within the current experimental uncertainty of ~ 5 GeV on m_t , but is in the range $\mathcal{O}(10^{-7} - 10^{-6})$, well beyond the sensitivity of the LHC or a LC.

3.1.2 Neutral current decays

With current experimental input, the SM predicts $\mathcal{B}(t \rightarrow cg) \sim 4 \times 10^{-13}$, $\mathcal{B}(t \rightarrow c\gamma) \sim 5 \times 10^{-13}$, and $\mathcal{B}(t \rightarrow cZ) \sim 1 \times 10^{-13}$ (84). While $\mathcal{B}(t \rightarrow cH^0)$ depends on M_{H^0} , it also cannot exceed $\sim 10^{-13}$. These are all well below the detection limits of even the LHC or a LC (85). Direct searches for FCNC decays by CDF have set limits of $\mathcal{B}(t \rightarrow c\gamma) + \mathcal{B}(t \rightarrow u\gamma) < 0.032$ and $\mathcal{B}(t \rightarrow cZ) + \mathcal{B}(t \rightarrow uZ) < 0.33$ at 95% C.L. (15). These limits are dominated by statistical uncertainties, and are expected to improve by up to a factor 10 following Tevatron Run 2. The LHC experiments have also estimated their 5σ discovery reach for these processes.

Given a 100 fb^{-1} data sample, the minimum branching fractions accessible to ATLAS and CMS are in the vicinity of 2×10^{-4} for both $t \rightarrow Zq$ and $t \rightarrow \gamma q$ (18).

Rates are smaller still for $t \rightarrow cX_i^0 X_j^0$. Such FCNC decays can be significantly enhanced, however, in various scenarios beyond the SM.

3.2 Top quark decays beyond the Standard Model

Many channels emerge to compete with top quark SM decays in the presence of new physics. Extended Higgs sectors, alternative mechanisms for EWSB and mass hierarchies among supersymmetric particles all attach special significance to the top quark. We first consider minimal extensions to the SM Higgs sector without invoking any new symmetries. Special implications within the framework of the MSSM are dealt with following that, together with other scenarios suggested by SUSY. Finally, we examine topcolor-assisted technicolor (TC2).

3.2.1 Decays with an extended Higgs sector

The SM Higgs sector consists of a single complex scalar doublet. The single, neutral scalar Higgs boson that arises after EWSB does not affect top decays in any measurable way. However, with the addition of a second Higgs doublet comes charged Higgs states. If kinematically allowed, $t \rightarrow bH^\pm$ can have a significant branching fraction. This is important not merely because a richer Higgs sector is experimentally allowed, but because it is in fact required by some of the leading candidates for new physics. The simplest extension is to two complex scalar doublets, generically called two-Higgs double models (2HDM). In this case, EWSB results in five physical Higgs bosons: two neutral scalars (h, H), a neutral pseudoscalar (A), and a pair of charged scalars (H^\pm). Two new

parameters enter at tree level, usually taken to be M_A or M_{H^\pm} , and $\tan \beta \equiv \frac{v_2}{v_1}$, where v_i are the vacuum expectation values of the Higgs fields ϕ_i ($i = 1, 2$). Both charged and neutral Higgs boson can appear in tree-level top decays, the latter implying FCNCs.

Decays to charged Higgs bosons:

Among a few variants of the two-Higgs-doublet models (2HDM) is the ‘‘Type 2’’ model, where one doublet couples to up-type fermions and the other to down-type. This is required, for example, in the MSSM (86).

If $M_{H^\pm} < m_t - m_b$, then

$$\Gamma(t \rightarrow H^\pm b) \propto (m_t^2 \cot^2 \beta + m_b^2 \tan^2 \beta)(m_t^2 + m_b^2 - M_{H^\pm}^2) + 4m_t^2 m_b^2 \quad (3)$$

at tree level. For fixed M_{H^\pm} , this function is symmetric in $\log(\tan \beta)$ about a minimum at $\tan \beta = \sqrt{\frac{m_t}{m_b}}$. For given $\tan \beta$, the partial width decreases as M_{H^\pm} increases. If one ignores fermion masses except when they are multiplied or divided by $\tan \beta$, then in the diagonal CKM approximation the fermionic decay partial widths are given by

$$\Gamma(H^\pm \rightarrow U\bar{D}) = \frac{N_c g^2 M_{H^\pm}}{32\pi M_W^2} (m_U^2 \cot^2 \beta + m_D^2 \tan^2 \beta), \quad (4)$$

where $U[D]$ is an up-[down-] type fermion and $N_c = 1[3]$ for leptons [quarks]. With the current experimental lower limit of $M_h > 91.0$ GeV and $M_A > 91.9$ GeV at 95% C.L. (87), bosonic decays $H^\pm \rightarrow W^\pm h, W^\pm A$, are kinematically suppressed for $M_{H^\pm} < m_t - m_b$.

Thus, for $\tan \beta > 1$, $H^\pm \rightarrow \tau\nu_\tau$ is the dominant decay channel. If $\tan \beta < 1$, the decay depends on M_{H^\pm} : for $M_H^\pm \approx 100$ GeV, $H^\pm \rightarrow cs$ and $H^\pm \rightarrow bc$ compete more or less evenly (CKM suppression due to $|V_{cb}| \ll |V_{cs}|$ is offset by the stronger H^\pm coupling to b relative to s); but as M_H^\pm is increased beyond 120

GeV, weight gradually shifts to $H^\pm \rightarrow Wbb$ via a virtual top quark. Strategies for H^\pm searches therefore depend on M_{H^\pm} and $\tan\beta$. Searches for $e^+e^- \rightarrow H^+H^-$ at LEP constrain $M_{H^\pm} > 78.6$ GeV at 95% C.L. (88), while the CLEO experiment has set a limit of $M_{H^\pm} > (244 + 63/(\tan\beta)^{\frac{1}{3}})$ GeV at 95% C.L. from the inclusive measurement of $b \rightarrow s\gamma$ (89).

By itself, an extended Higgs sector does not significantly alter $\sigma_{t\bar{t}}$ at hadron colliders. One looks instead for either the appearance of $t \rightarrow H^\pm b$ signatures or, indirectly, disappearance of the SM $t \rightarrow Wb$ signatures. For the latter, one assumes $\mathcal{B}(t \rightarrow H^\pm b) + \mathcal{B}(t \rightarrow Wb) = 1$. Both CDF and DØ conducted searches for $t \rightarrow H^\pm b$ in $p\bar{p} \rightarrow t\bar{t}$ events in Run 1 (13, 14). Figure 8 shows the DØ results from their disappearance search together with projections for Run 2.

The direct searches focused on $H^\pm \rightarrow \tau\nu$. With good τ identification capability, this can yield the strongest results, albeit limited to $\tan\beta > 1$, where the process has a large branching fraction. Combinations of different methods and of data from the two experiments may indeed eventually give stronger constraints. As expected, searches are more difficult in the region around $\tan\beta = \sqrt{\frac{m_t}{m_b}}$, where $t \rightarrow bH^\pm$ is highly suppressed. Searches for $H^\pm \rightarrow cs, cb$ are made more challenging by overlap with the SM decay $t \rightarrow Wb \rightarrow q_1q_2b$. However, a dijet invariant mass peak between 110 GeV and 130 GeV corresponding to M_{H^\pm} is a viable signal for Tevatron Run 2 and LHC. For $M_{H^\pm} > 130$ GeV, $t \rightarrow bH^\pm \rightarrow Wbbb$ may offer cleaner signatures, but $\mathcal{B}(t \rightarrow bH^\pm)$ decreases rapidly with increasing M_{H^\pm} . Increased statistics from Run 2 and the LHC will push the exclusion contours asymptotically closer (see Fig. 8) - or perhaps the process will be observed. The exclusion boundaries in the $[M_{H^\pm}, \tan\beta]$ plane roughly follow contours of constant $\mathcal{B}(t \rightarrow bH^\pm)$. Thus, 95% C.L. upper limits on $\mathcal{B}(t \rightarrow bH^\pm)$ for $\tan\beta > 1$

(where $H^\pm \rightarrow \tau\nu$ dominates) are 0.36 from $D\bar{O}$ and 0.5-0.6 from CDF. The disappearance search result from $D\bar{O}$ can be interpreted as $\mathcal{B}(t \rightarrow bH^\pm) < 0.45$ at 95% C.L., irrespective of $\tan\beta$ except in the region where $H^\pm \rightarrow Wbb$ is the dominant decay mode (i.e. when $\tan\beta < 1$ and $M_{H^\pm} > 125$ GeV). The corresponding estimate for Run 2 is $\mathcal{B}(t \rightarrow bH^\pm) < 0.11$ at 95% C.L. (90).

All H^\pm searches hinge on the fact that, unlike for W^\pm , H^\pm fermion couplings are not flavor-blind. This implies we should compare the values for $\sigma_{t\bar{t}}$ derived from different final states, based on the SM assumption of $\mathcal{B}(t \rightarrow Wb) \approx 1$. For example, if the dilepton, single-lepton, and all-jets $t\bar{t}$ final states exhibited differences, it could indicate significant alternative decay modes to $t \rightarrow Wb$. While less restrictive in assumptions, this method also yields the least stringent conclusions. Tevatron Run 1 data is statistically insufficient for a meaningful application of this method, but that will change for Run 2 and the LHC.

FCNC decays in a 2HDM:

FCNC top quark decay rates can be enhanced if one abandons the discrete symmetry invoked in the Type 2 2HDM to suppress tree-level scalar FCNCs. In the more general Type 3 2HDM, fermions are allowed to couple simultaneously to more than one scalar doublet (91)⁸. Single vector-boson FCNC decays, $t \rightarrow cV_i^0$ ($V_i^0 = \gamma, Z, g$) are still loop-induced, as shown in Fig. 9(a,b), but can have branching fractions as large as $\mathcal{O}(10^{-5})$ even without any new interactions⁹. Double vector-boson FCNC decays, $t \rightarrow cV_i^0V_j^0$ also appear at the tree-level (Fig. 9(c)), and can reach branching fractions of $\mathcal{O}(10^{-5})$ (92).

With production rates of $\mathcal{O}(10^3 - 10^4)$ per year (see Table 1), such events

⁸Low energy limits on FCNCs may be explained by tuning of the Yukawa matrices.

⁹These branching fractions can be enhanced by more than a factor 10 under favorable conditions in the MSSM.

could be studied at the LHC only if they are given high priority in triggering during high-luminosity running, because suppression of large SM backgrounds will translate into small signal efficiencies. At a LC, production rates are at most $\mathcal{O}(1 - 10)$ per year, but low background and very high ($\sim 90\%$) signal efficiency may make these processes observable, should they occur.

3.2.2 Supersymmetric decays of the top quark

In SUSY, the large Yukawa coupling of the top quark can lead to large mass splitting among the superpartners of the third generation fermions. The superpartners of the right-handed and left-handed top quark combine to form mass eigenstates \tilde{t}_1 and \tilde{t}_2 . The lightest top squark, \tilde{t}_1 , can be lighter than all other squarks, and in fact have mass near m_t . Naturally, this has implications for possible top decays. We first address top SUSY decays under the assumption that \mathcal{R} -parity¹⁰ is conserved. Afterward, we drop this assumption.

\mathcal{R} -parity conservation requires superparticles to be produced in pairs and forbids decays of the lightest SUSY particle (LSP). The LSP is widely assumed to be the lightest neutralino, $\tilde{\chi}_1^0$ (neutralinos are the sfermion partners of the SM bosons). Under this assumption, the most likely top SUSY decay is $t \rightarrow \tilde{t}_1 \tilde{\chi}_1^0$. Generally, the top squark will decay via $\tilde{t}_1 \rightarrow c \tilde{\chi}_1^0$ or $b \tilde{\chi}_1^+$, depending on the various daughter masses. In the latter case, $\tilde{\chi}_1^+ \rightarrow \tilde{\chi}_1^0 \ell \nu_\ell$ or $\tilde{\chi}_1^0 q_1 \bar{q}_2$. The neutralinos interact only weakly, so generally escape without detection like neutrinos.

Branching fractions as large as 0.4-0.5 are possible for $t \rightarrow \tilde{t}_1 \tilde{\chi}_1^0$ (93). In such a scenario, about one half of $t\bar{t}$ events would have one SM and one SUSY top decay.

The CDF experiment has searched Run 1 data for events of this type where the

¹⁰A discrete, multiplicative symmetry defined as $\mathcal{R}_p \equiv (-1)^{3B+L+2S}$, where B is baryon number, L lepton number, and S spin.

SM top decay proceeds as $t \rightarrow Wb \rightarrow \ell\nu_\ell b$ ($\ell = e, \mu$), while the SUSY decay of the other top proceeds as $t \rightarrow \tilde{t}_1\tilde{\chi}_1^0 \rightarrow b\tilde{\chi}_1^+\tilde{\chi}_1^0 \rightarrow bq_1\bar{q}_2\tilde{\chi}_1^0\tilde{\chi}_1^0$. The signal consists of a lepton, \cancel{E}_T , and 4 jets (including the two b -jets): identical to SM single lepton decay, but differing in p_T and angular distributions. These depend on the masses of the particles involved. Based on the assumptions $\mathcal{B}(\tilde{\chi}_1^\pm \rightarrow \ell\nu\tilde{\chi}_1^0) = \frac{1}{9}$, $\mathcal{B}(\tilde{t}_1 \rightarrow b\tilde{\chi}_1^\pm) = 1$, and $\mathcal{B}(t \rightarrow \tilde{t}_1\tilde{\chi}_1^0) + \mathcal{B}(t \rightarrow Wb) = 1$, the search excluded $\mathcal{B}(t \rightarrow \tilde{t}_1\tilde{\chi}_1^0) > 0.45$ at 95% C.L. over most of the kinematically allowed portion of the $[m_{\tilde{t}_1}, m_{\tilde{\chi}_1^\pm}]$ parameter space for $m_{\tilde{\chi}_1^0}$ up to 40 GeV (94). For larger LSP masses, the kinematically allowed region shrinks.

The alternative scenario, $t \rightarrow \tilde{t}_1\tilde{\chi}_1^0 \rightarrow c\tilde{\chi}_1^0\tilde{\chi}_1^0$, is similar in character to the FCNC decay $t \rightarrow cZ \rightarrow c\nu\nu$. The most promising channel is where one top undergoes the non-SM decay while the other follows the SM. If the W decays leptonically, then the signal consists of a high- p_T isolated lepton, substantial \cancel{E}_T , and 2 jets, one of which is a b . The large background from $W(\rightarrow \ell\nu) + \geq 2$ jets limits the search to regions of parameter space where $m_{\cancel{E}_T} > M_W$. If, on the other hand, the W decays hadronically, then we have 4 high- p_T jets and large \cancel{E}_T for signal. Backgrounds arise chiefly from $W(\rightarrow \tau\nu) + \geq 3$ jets events where the τ is misidentified as a jet, and from $Z(\rightarrow \nu\nu) + \geq 4$ jets. Effectiveness of b -tagging is reduced since there is only one b -jet per event. Sensitivity is further compromised in much of the $[m_{\tilde{t}_1}, m_{\tilde{\chi}_1^0}]$ parameter space where the jet and \cancel{E}_T spectra are soft and/or broad. Tevatron Run 1 data was statistically insufficient for this analysis, but that will change in Run 2.

\mathcal{R} -parity violating (\mathcal{R}_p) interactions in the MSSM greatly enhance FCNCs (95). Within a single coupling scheme, either the up-type quarks or the down-type quarks can avoid these processes, but not both simultaneously. The consequences

of \mathcal{R}_p have been studied via measurements of K^0 - \bar{K}^0 , D^0 - \bar{D}^0 and B^0 - \bar{B}^0 mixing, and of $\mathcal{B}(K^+ \rightarrow \pi^+ \nu \bar{\nu})$, resulting in constraints on the $j = 1, 2$ elements of the $3 \times 3 \times 3$ \mathcal{R}_p coupling matrix λ'_{ijk} (i, j, k are generation indices), but leaving the third generation somewhat unconstrained. If sleptons lighter than the top quark exist, then $t_L \rightarrow d_{Rk} \tilde{\ell}_i^+$ followed by $\tilde{\ell}_i^+ \rightarrow \tilde{\chi}_0 \ell_i$ and $\tilde{\chi}_0 \rightarrow \bar{\nu}_i \bar{b} d_k$ can lead to a fairly clean signature (\mathcal{R}_p implies that the $\tilde{\chi}_0$, assumed here to be the LSP, is not stable). Future searches for such signals will constrain λ'_{i3k} ($k \neq 3$).

3.2.3 Top decays in topcolor-assisted technicolor

In technicolor theories (96), EWSB is accomplished by chiral symmetry breaking of technifermions which transform nontrivially under a new strong gauge interaction called technicolor (TC). This yields correct weak boson masses if the scale of technicolor interactions is about a TeV. Fermion masses arise without fundamental scalars, by invoking an additional, spontaneously broken gauge interaction called extended technicolor (ETC) (97). However, ETC interactions cannot account for the large mass of the top quark (98).

Topcolor-assisted technicolor (TC2) is an attempt to address this deficiency (61). In the simplest version, the third generation is assumed to transform with the usual quantum numbers under strong $SU(3)_h \times U(1)_h$, while the lighter generations transform identically under a different (weaker) group $SU(3)_l \times U(1)_l$. At scales of about 1 TeV, $SU(3)_h \times SU(3)_l$ and $U(1)_h \times U(1)_l$ spontaneously break down to ordinary color $SU(3)_C$ and weak hypercharge $U(1)_Y$, respectively. EWSB is still driven primarily by TC interactions, but topcolor interactions, felt only by the third generation quarks (also at a scale near 1 TeV), generate the very large top quark mass. ETC interactions are still required to generate the

light fermion masses and a small but important contribution to the mass of the top quark m_t^{ETC} . The reason for a nonzero m_t^{ETC} is to give mass to the *top-pions*, the Goldstone bosons of t, b chiral symmetry breaking.

In TC2 models, the $tb\pi_T^+$ coupling is small, but the $tb\pi_t^+$ coupling is large, and the ETC interactions responsible for the small component of m_t induce mixing between top-pions and technipions. The consequence is a possibly significant partial width (if kinematically allowed):

$$\Gamma(t \rightarrow \pi_t^+ b) = \frac{|\epsilon|^2}{16\pi} \left(\frac{m_t^{\text{dyn}}}{m_t} \right)^2 \frac{(m_t^2 - m_{\pi_t}^2)^2}{F_t^2 m_t}, \quad (5)$$

where ϵ is the top-pion component of the technipion mass eigenstate, m_t^{dyn} the dynamical top quark mass, m_{π_t} the technipion mass, and F_t (≈ 70 GeV) the top-pion decay constant. Short of direct discovery, a precise experimental determination of Γ_t is required to limit the allowed parameter space in these models.

4 Top Quark Properties

Confirmation of the SM nature of the top quark requires that we measure all its quantum properties and compare with SM expectations. Deviations would indicate new physics. In this section we describe the status and future expectations of these measurements, and the crucial issues in making them.

4.1 Mass

While the top quark is the least well-studied quark in terms of quantum properties, its mass, m_t , is more accurately known (as a fraction of its mass) than any other quark. This is also extremely important, as the top quark's role in SM precision fits is proportionally more important than any other. This is an artifact of EWSB and the large value of the top Yukawa coupling, Y_t . That Y_t appears to

be exactly one has not gone unnoticed. Proponents of strong dynamical EWSB argue it that supports this class of theories, because in general they predict large values of Y_t , on the order of 1 or more. On the other hand, it is also generally regarded as support for SUSY extensions to the SM, which would not be viable unless the top quark mass were large: the running of $\sin^2 \theta_W$ could not be made to fit the data and still allow for gauge coupling unification otherwise, and EWSB would not occur, since the large value of the top Yukawa coupling is what drives the coefficient of the Higgs mass term negative. But large m_t does not point at either class of theories as the clear favorite. One is left with the simple suspicion that the top quark is perhaps connected to new physics on the grounds that physical parameters of exactly 1, (or 0, etc.) indicate a more fundamental property underlying Y_t .

The impact of m_t elsewhere varies. In B and K physics, many observables have terms roughly quadratic in $\frac{m_t}{M_W}$. It was, in fact, data from $B_0 - \bar{B}_0$ mixing in 1987 that first indicated a heavy top quark. For precision SM EW fits, m_t enters quadratically in many places as well. Examples are R_b , A_{LR} , $\sin^2 \theta_W$ and the parameter $\rho \equiv \frac{M_W^2}{M_Z^2 \sin^2(\theta_W)}$. The corrections usually appear as a multiplicative factor, $1 + \frac{3G_F m_t^2}{8\sqrt{2}\pi^2}$. The W mass, which is not known nearly as precisely as most of the other quantities in the EW sector, receives quantum corrections proportional to m_t^2 and $\ln(M_H)$, where M_H is the Higgs boson mass. This is usually plotted as m_t v. M_W , overlaid with bands that show the predicted M_H , as in Fig 1. A “light” Higgs is favored, somewhere around 100 GeV, but with an uncertainty also of $\mathcal{O}(100)$ GeV. Unfortunately, as the M_H dependence is only logarithmic, and in the presence of new physics this fit is not meaningful unless the new physics is also known precisely, one cannot draw firm conclusions from these fits. As the

precision of m_t and M_W increases, however, and if a Higgs remains unobserved, the fit increasingly suggests breakdown of the SM.

The current precision of B and K physics is not good enough to require better precision in m_t than is available from Tevatron Run 1, but the next generation of K experiments will need $\delta m_t \simeq 3\% \simeq 5$ GeV, which should be satisfied by Run 2. The EW precision fits are more demanding. Once the W mass precision reaches 20 MeV at the LHC, m_t must be known within 3 GeV to not limit the EW precision fit for M_H . For a future linear collider, the 6 MeV precision on M_W must be matched by 1 GeV precision in m_t .

Both the LHC and a LC can outperform these goals: at the LHC, $\delta m_t \simeq 2$ GeV is expected within 1 year of low-luminosity running, while 1 GeV could be achieved with the $\ell J/\psi$ final state (discussed shortly) and a larger data set (18). Precision of $\mathcal{O}(100$ MeV) can be obtained at a future linear collider with a $t\bar{t}$ threshold scan (99), which does not measure the pole mass and so is not limited by uncertainties of $\mathcal{O}(\Lambda_{QCD})$.

One specific case where super-precision of m_t would be necessary is if low-energy SUSY is found. In the MSSM, the mass of the lighter CP-even neutral Higgs boson h is given at the NLO by

$$M_h^2 = M_Z^2 + \frac{3G_F}{\pi^2\sqrt{2}} m_t^4 \ln\left(\frac{M_S^2}{m_t^2}\right), \quad (6)$$

where M_S^2 is the average of the two top squark squared masses. Since a LC could measure M_h to about 50 MeV precision (99), m_t would need to be known to 100 MeV or better to perform meaningful SUSY-EW precision fits. Ironically, this would require M_h to be known to probably the four-loop level; only two-loop calculations are currently available. One is forced to wonder if the requisite improvement in theoretical precision in that case would be realistic.

We now highlight the principles behind top mass measurements made so far at the Tevatron. Details and subtleties can be found in e.g. Refs. (100, 18, 101, 4, 5, 6, 8). The main idea is to compare the observed kinematic features of $t\bar{t}$ pairs to those predicted for different top quark masses. While many kinematic variables are sensitive to m_t , explicit reconstruction from the $t\bar{t}$ decay products is an obvious choice, as long as we understand that it is uncertain to at least $\mathcal{O}(\Lambda_{QCD})$. However, more elaborate methods that attempt to connect many observables simultaneously with the matrix elements of the production and decay processes on an event-by-event basis are gradually emerging as a superior alternative.

There are three channels to consider, depending on how the two top quarks decay: dilepton, single-lepton, and all-hadronic. Here, “lepton” refers to e, μ only, since the presence of additional neutrinos in τ decays severely limits the usefulness of $t\bar{t} \rightarrow \tau X$ channels in the m_t determination. Thus, the branching fractions of the three channels are approximately 0.05, 0.30 and 0.44, respectively. Signal and background characteristics vary from channel to channel, so the exact technique used must be tailored accordingly for each channel.

For direct reconstruction of invariant masses of the two top quarks in a $t\bar{t}$ candidate event, one needs to know the 4-momenta of the 6 daughters, a total of 24 quantities. Imagine an ideal $t\bar{t}X$ event with no final state radiation and where the momentum of X , which represents everything recoiling against the $t\bar{t}$ system, is fully measured. If the 3-momenta of n of the six final state objects are directly measured, we have $3n$ measured quantities from the two top decays. The masses of the 6 decay products are known (these can be safely assumed zero), as are the two intermediate W masses. Although m_t is yet unknown, it must be the same

for both tops in the event. So, we have 9 constraints from particle masses¹¹. That the $t\bar{t}X$ system carries no significant momentum transverse to the beamline gives two additional constraints¹²: $\vec{p}_T(t\bar{t}X) = 0$. Thus, a kinematic mass fit is subject to $(3n + 9 + 2 - 24) = (3n - 13)$ constraints. For each leptonic W decay, there is a corresponding neutrino that cannot be directly observed. Therefore, $n = 6$ for all-hadronic, $n = 5$ for single-lepton, and $n = 4$ for dilepton events. Dilepton events are underconstrained ($-1C$), preventing explicit m_t reconstruction from its daughters, forcing one to seek alternative means.

In every channel, many factors complicate m_t measurement. The observed objects' momenta need to be corrected to remove detector effects. The lion's share of the uncertainty in these corrections is due to jet energy measurements. Any sampling calorimeter has a relatively large inherent uncertainty in its absolute energy scale. Moreover, the detector geometry has non-uniformities such as module boundaries and gaps or "cracks" to allow passage of cables and other hardware. Therefore, the response must be carefully mapped as a function of the physical location of where the jet traversed the detector. It is often a non-linear function of jet energy. Additionally, each element of a calorimeter, or *cell*, has a minimum threshold to register energy. Reconstruction of jets proceeds through identification of clusters of (nearly) contiguous cells registering energy. These effects usually result in leakage that needs to be corrected for. Two other effects come from the nature of hadron collider events. In each $t\bar{t}$ hard scattering there is an associated *underlying event* from the proton/antiproton remnants, that deposits soft energy through the calorimeters. Also, in high luminosity running, each $t\bar{t}$ event is accompanied by *multiple interactions*, dominated by soft inelastic $p\bar{p}$ or

¹¹One has to appropriately allow for Γ_W and Γ_t .

¹²In general, $x_1 \neq x_2 \Rightarrow p_z(t\bar{t}X) \neq 0$.

pp scattering, that contribute to energy measurement contamination.

Other complications arise, more related to the physics of the $t\bar{t}$ event itself. One is that we often find jets that do not even originate from top decays directly, rather from initial or final state radiation (102). Due to detector segmentation or limitations in the reconstruction algorithms, two or more jets can get merged and reconstructed as one. Sometimes the opposite occurs: a single jet splits in two due to fragmentation. Occasionally, a jet is lost entirely because it travels through an uninstrumented or poorly instrumented region, such as the beampipe. These extra or missing jets result in admission of extraneous solutions into reconstructed m_t distributions.

Since the all-hadronic channel has a large branching fraction and is maximally constrained, one might surmise that it would be the best for measuring m_t . In practice, however, a very large and hard-to-model QCD multijet background, compounded by the jet measurement issues mentioned above, leads to relatively large uncertainties. The top mass extracted by CDF (103) in the all-hadronic channel is $186.0 \pm 10(\text{stat.}) \pm 5.7(\text{syst.})$ GeV. Each event is required to have six or more jets, and to satisfy several topological requirements that help improve the signal to background ratio. Events were reconstructed to the $t\bar{t} \rightarrow W^+bW^-\bar{b} \rightarrow q_1\bar{q}_2bq_3\bar{q}_4\bar{b}$ hypothesis using the six highest E_T jets, one of which must be b -tagged. This still leaves 30 different reconstruction combinations. A kinematic fit constrains each combination to yield M_W for two jet pairs, equal t and \bar{t} masses, returning a χ^2 value. The combination with the smallest χ^2 is chosen. The resulting “reconstructed mass” distribution from the candidate events is then compared, through a likelihood fit, to templates formed from the right mix of $t\bar{t}$ (from simulation) and QCD background, the shape of which is

extracted from data. The input m_t is changed and the value that maximizes the likelihood L is the central value of the top mass measurement. The statistical uncertainty is determined from the range over which the $-\ln L$ increases by $\frac{1}{2}$ unit with respect to its minimum. An analysis of the all-hadronic final state recently completed by DØ is similar in spirit, but employs an artificial neural network algorithm to compensate for a lower b -tagging efficiency. The preliminary result is $176^{+17.1}_{-13.6}$ GeV.

The ultimate precision achievable in this channel is not expected to rival that of the single-lepton or dilepton channels but can still be used in a combined result to help reduce the overall uncertainty. A top mass measurement in this channel is important on its own merits because it confirms that the excess of tagged 6-jet events indeed comes from top, or at least from a particle with a mass consistent with that measured in the other decay modes. Analysis of this final state is not very likely to be feasible at the LHC.

In addition to an isolated high- p_T electron or muon in the central region of the detector, a single-lepton candidate event is required to have at least four jets in order to perform a kinematical fit to the top mass by a method similar to the one discussed above. Here the sample is much cleaner but still suffers from combinatorial ambiguities in the reconstruction. Including the two-fold ambiguity in the neutrino p_z , it is four-fold if both b jets are tagged, 12-fold if only one b is tagged and 24-fold if none is. Run 1 results in this channel are $173.3 \pm 5.6(\text{stat.}) \pm 5.5(\text{syst.})$ [DØ (4)] and $176.1 \pm 5.1(\text{stat.}) \pm 5.3(\text{syst.})$ [CDF (8)].

It is interesting to note that even for the case when both b -jets are tagged, MC simulations suggest that in only about half of the cases does the best χ^2 correspond to the correct matching of the four leading jets to the appropriate

quarks. The other half are roughly equally split between instances where all jets are matched to partons, but the lowest χ^2 did not choose the combination with the correct assignments, and those where there are extra jets from initial or final state radiation and the four leading partons from the $t\bar{t}$ decay cannot be uniquely matched to the four leading jets in the event. At the LHC, $t\bar{t}$ events will have higher p_T , on average. This will often mean that the daughters of the two tops will be on opposite sides of a plane. Such hemispheric separation will considerably alleviate these combinatorial problems.

A more recent analysis in the single-lepton channel by DØ (5) makes a comparison of data with LO matrix elements on an event-by-event basis, similar to that suggested (104,80) and used for the dilepton channel discussed below. This analysis requires the number of jets in a candidate event to be exactly 4, and does not accord any special status to events with b -tagged jets. A likelihood function is formed taking into account all possible permutations of jet assignments, not just that with the lowest χ^2 . The main difference between this method and the previous is that each event now has an individual probability as a function of m_t . This probability, reflecting both signal and background, depends on all measured variables in the event (except unclustered energy), with well-measured events contributing more sharply to the extraction of m_t than those poorly measured. The preliminary result, $m_t = 179.9 \pm 3.6(\text{stat.}) \pm 6.0(\text{sys.})$ GeV, reflects a marked reduction of the statistical uncertainty relative to the previous result, which was based on the same data set but relied heavily on explicit reconstruction of invariant masses.

Two alternatives to invariant mass reconstruction have been tried to measure m_t in the kinematically underconstrained dilepton channel, $t\bar{t} \rightarrow \ell_1\nu_1 b\ell_2\nu_2\bar{b}$,

which also suffers from the smallest branching fraction. In the first (104), one hypothesizes a mass for the top quark, reconstructs the neutrino momenta with a four-fold ambiguity for each lepton- b pairing, and calculates the probability of the final-state configuration to come from a $t\bar{t}$ event of that m_t . For each event, a set of assumed masses produces probability distributions to use as event weights. The preferred m_t for an event can be taken as the maximum or the mean of the distribution. The distribution of preferred masses for a set of candidate events is compared through a likelihood method to the expected distribution from a combination of signal and background, for given m_t . As in the other channels, the central value of the measurement is that with maximum likelihood.

Variants of this technique make use of more or fewer assumptions about $t\bar{t}$ production details when obtaining the event probabilities. For example, DØ has two different measurements, one using neutrino kinematic distribution weights and another that uses production and decay terms in the matrix element for the weights. The methods yielded very consistent results. The final result is (6, 100) $m_t = 168.4 \pm 12.3(\text{stat.}) \pm 3.6(\text{syst.})$.

CDF's measurement in the dilepton channel used only information about the expected pseudorapidity distributions of the neutrinos. These were chosen randomly from MC predictions, then the two neutrino momenta were solved for. Each solution (ambiguity included) was assigned a weight according to how well the derived \vec{E}_T matches that measured. CDF's result is (8, 100) $m_t = 167.4 \pm 10.3(\text{stat.}) \pm 4.8(\text{syst.})$. CDF also used a likelihood fit to kinematical variables that are sensitive to m_t : the b -jet energy spectrum and the full event invariant mass (105). Results from these are consistent, but suffer larger systematic uncertainties.

The other method for the dilepton channel (80) is based on the observation that, modulo finite W width effects, the b quark energy is fixed in the top quark rest frame. The top mass is then given by $m_t^2 = \langle m_{b\ell}^2 \rangle + \sqrt{M_W^4 + 4M_W^2 \langle m_{b\ell}^2 \rangle + \langle m_{b\ell}^2 \rangle^2}$, where $\langle m_{b\ell}^2 \rangle$ is the mean value of $m_{b\ell}^2$ in the sample. The results are generally consistent with the likelihood methods.

The dilepton sample also contains a subsample of events that may prove useful at the LHC for improving its uncertainties. Here, one looks for events where one of the b quarks hadronizes to J/Ψ , which subsequently decays to $\ell^+\ell^-$, providing a cleaner and more precisely measured sample. When the sister W decays leptonically to $\ell'\nu_{\ell'}$, a strong correlation exists between m_t and $m_{J/\Psi\ell'}$ (106). The top mass can be extracted essentially from the end point of the Gaussian $m_{J/\Psi\ell'}$ distribution. In recent improvements to HERWIG, matrix element corrections to radiative top decays are known to cause a 1-1.5 GeV shift in the extracted m_t (107). Study of this endpoint spectrum is ongoing, and must take into account this MC improvement, to attain the goal of 1 GeV precision in this channel.

The Tevatron average for m_t is $174.3 \pm 3.2(\text{stat.}) \pm 4.0(\text{syst.})$ (7). Fig. 10 shows the breakdown per channel, and the global average. Table 3 summarizes the systematic uncertainties in the DØ and CDF Run 1 m_t measurements in the various channels. As mentioned above, most of the systematic uncertainty comes from the jet energy scale. Experiments need to understand and maintain the calibration of their calorimeters to high precision to help keep part of this systematic under control.

With larger samples of events in Run 2 and at the LHC, both statistical and systematic uncertainties will be reduced significantly. There are several reasons for this. First, one can afford to narrow the focus to samples with two b -tagged

jets. This reduces combinatorics, but also energy scale uncertainty, since specific energy corrections to b -jets can be applied to help with the mass resolution. One can also choose specific subsets of events in which, for example, the exact number of jets as expected from top are found and in which the jet energies are particularly well measured (be it fiducially or due to high energy). Events with particular topologies can similarly help. ATLAS and CMS plan to use angular information and possible hemispheric separation of the two top quarks as well, to assist with correct $b - W$ combination. Additionally, with large integrated luminosity samples, the control samples used to map the calorimeters' energy responses, such as photon+jets and high- E_T di-jets, will be less statistically limited and will help reduce the jet energy scale uncertainty.

Another source of improvement in the mass measurement can come from a better understanding of the treatment of initial and final state radiation. If the parton came from initial state radiation, including it in the reconstruction would bias m_t toward larger masses. If it instead came from radiative top decay or the final state b quark, it must be included, else m_t is measured to be too low. This issue has been known for a long time, and addressed at the theoretical level with exact calculations of the expected rates for and radiation patterns of one additional hard parton (34). These authors propose to assign additional hard jets in events to either production or decay by calculating the following observables:

$$S_{prod} = |[(p_{W^+} + p_b)^2 - m_t^2 + im_t\Gamma_t] \times [(p_{W^-} + p_{\bar{b}})^2 - m_t^2 + im_t\Gamma_t]| \quad (7)$$

$$S_1 = |[(p_{W^+} + p_b)^2 - m_t^2 + im_t\Gamma_t] \times [(p_{W^-} + p_{\bar{b}} + p_j)^2 - m_t^2 + im_t\Gamma_t]| \quad (8)$$

$$S_2 = |[(p_{W^+} + p_b + p_j)^2 - m_t^2 + im_t\Gamma_t] \times [(p_{W^-} + p_{\bar{b}})^2 - m_t^2 + im_t\Gamma_t]| \quad (9)$$

The extra jet is “production” if $S_{prod} < \min(S_1, S_2)$, and “decay” otherwise; this

assumes of course that in samples containing hadronic W decays, the correct assignment has already been made for the W jets (i.e. a radiative W decay could be identified). How well the idea may apply under experimental constraints remains to be evaluated.

4.2 Spin

All SM fermions have a left-handed weak gauge coupling, which mediates their decays, if they decay. Only the top quark, because it is so massive, decays before it hadronizes or its spin flips, thus leaving an imprint of its spin on its angular decay distributions. But how do we even know that the top quark candidate is a fermion? First, if it were spin 0 or 1, we would have to postulate an additional unobserved daughter to conserve overall spin. Furthermore, although Tevatron and LHC use unpolarized beams and therefore produce unpolarized top quark pairs, for spin 0 their spins would be uncorrelated, whereas for spin 1 they would be, although this correlation has not been considered. The spin correlations arising from a spin 3/2 scenario have also not been considered. However, a simple argument against spin 3/2 is that the $t\bar{t}$ cross section would be much larger. This was in fact how the tau lepton was determined to be spin 1/2.

As a spin 1/2 fermion, the SM top quark has decay angular distributions $d\Gamma/d(\cos\theta_i^*) \propto 1 + \alpha_i \cos\theta_i^*$, where θ_i^* is the angle of decay particle i in the top quark rest frame with respect to the top quark spin ($i = \ell^+, \nu, b$, or \bar{d}, u, b), and α_i is the *spin analyzing power* of particle i . At LO, $\alpha_i = 1, -0.32, -0.41$ (α_i have opposite signs for top quark and anti-top quark), making the outgoing charged lepton or down-type quark not tagged as a b the ideal spin correlation analyzer. If one uses the down-type quark in hadronic W decays, the QCD NLO corrected

value must be used (108): $\alpha_{\bar{d}} \simeq 0.93$. For top quark pair production, because the spins are correlated, one plots a double differential distribution (109, 110),

$$\frac{1}{\sigma} \frac{d^2\sigma}{d(\cos\theta_i)d(\cos\theta_{\bar{i}})} = \frac{1}{4}(1 - C \alpha_i \alpha_{\bar{i}} \cos\theta_i \cos\theta_{\bar{i}}), \quad (10)$$

where $\theta_i(\theta_{\bar{i}})$ is now the angle of the $i^{\text{th}}(\bar{i}^{\text{th}})$ decay product with respect to the chosen spin axis in the top (anti-top) quark rest frame; and C is the *spin correlation coefficient* - the relative fraction of like-spin top quarks produced, in the spin basis considered. Near threshold, $t\bar{t}$ produced by quark pairs is in a 3S_1 state, whereas gluon production yields a 1S_0 state, so the two components will have different spin correlations, $C_{q\bar{q}}$ and C_{gg} . Observing the overall correlation would confirm that the top quark is indeed the SM partner of the bottom quark with a left-handed weak coupling.

The overall spin correlation coefficient C varies strongly depending on spin basis and which initial state parton type dominates. Because $t\bar{t}$ production at the Tevatron is predominately quark-initiated, while at the LHC it arises mostly from initial gluons, different spin bases optimize analyses for the two machines. At the Tevatron this is the “off-diagonal” basis of Ref. (110), where the spin basis angle ψ with respect to the proton beam direction is a function of the speed and production angle θ_t of the top quark with respect to the incoming p direction in the zero momentum frame (ZMF):

$$\tan\psi = \frac{\beta^2 \sin\theta_t \cos\theta_t}{1 - \beta^2 \sin^2\theta_t}. \quad (11)$$

This basis is illustrated in Fig. 11 (110). At the LHC, the “helicity basis” is optimal, which resolves spin along the flight direction of the top quarks in the ZMF. The NLO corrections to C are known to be $\mathcal{O}(10\%)$, and so will not greatly affect an analysis (111). However, the uncertainty in C even at NLO is

unexpectedly large at the Tevatron. Because C_{gg} contributes with opposite sign to $C_{q\bar{q}}$, the overall value is quite sensitive to uncertainties in the gluon structure function at high x . Thorough study of PDF uncertainties will be required to resolve this. It is not as serious an issue at the LHC, as this process probes $g(x)$ at low x , where the PDF uncertainties are quite small, and in any case the scale uncertainty at NLO dominates over PDF uncertainties for this machine. At the Tevatron in the off-diagonal basis, $C_{NLO} = 0.806^{+2.9\%(\mu)}_{-4.0\%(\mu)}^{+4.0\%(\text{PDF})}_{-8.9\%(\text{PDF})}$, and in the helicity basis at the LHC, $C_{NLO} = 0.311^{+6.4\%(\mu)}_{-10.6\%(\mu)}^{+6.8\%(\text{PDF})}_{-0.0\%(\text{PDF})}$ (111).

Because the spin analyzing power of the charged lepton (leptonic decay) or d quark (hadronic decay) is maximal, they are the natural choice for observing the correlations. The dilepton $t\bar{t}$ sample has the least background contamination, but because of the two missing neutrinos can be reconstructed only statistically. Flavor tagging is not possible among the light quarks, but the down-type quark is typically the least-energetic quark in W decay in the top quark rest frame. In principle, then, use of the single-lepton and all-hadronic channels is possible, but needs further investigation.

If the top quarks decay isotropically, then $C = 0$ (no correlation). New physics such as CP violation or a right-handed coupling component would also alter the predicted value of C (112). The task then is to determine the achievable level of uncertainty on C at Tevatron and LHC. DØ has performed an analysis of their dilepton samples (10). While the statistics were too poor to give a strong result, they clearly established that the measurement can be performed. Run 2 expectations are that $C = 0$ can be ruled out at better than the 2σ level with 2 fb^{-1} of data. At the LHC, CMSJET simulation (18) estimates a measurement of $C = 0.331 \pm 0.023$ (statistical errors only, LO simulation) for the

SM, more than good enough to rule out the isotropic decay case. Polarimetry of the b quark has been proposed to enhance spin correlation analyses (113), but has not yet been investigated by the experimenters. Of course, the ultra-low background environment, beam polarization, and \sqrt{s} tuning of a LC would be ideal for precision spin and spin correlation measurements (114).

Because all three modes of single top quark production (Fig. 6) can be observed at both Tevatron and LHC, it is useful to consider spin for these cases as well. Here the interesting distribution is the angle θ between the charged lepton in the top quark decay and the chosen spin axis (115, 116):

$$\frac{1}{\sigma_T} \frac{d\sigma}{d\cos\theta} = \frac{1}{2} \left[1 + C' \cos\theta \right], \quad C' = \frac{N_{\uparrow} - N_{\downarrow}}{N_{\uparrow} + N_{\downarrow}}. \quad (12)$$

where $N_{\uparrow(\downarrow)}$ is the number of top quark events produced spin up (down) in the frame considered. The spin asymmetry C' in this case is maximized by choosing the spin basis that most strongly correlates with the down-type quark on the production side. For W^* production, this is simply the antiproton direction at the Tevatron (115). The Wg -fusion process is more challenging due to NLO complications in the initial and final states as the ZMF cannot be defined. Here one optimally chooses the “ η -beamline” basis, which is defined as the beamline most closely aligned with the forward scattered quark that supplied the fusing W (115). For Wt production the ideal basis is defined by the down-type fermion from both W decays (116). This channel has severe experimental problems reconstructing the top quark rest frame for most decay channels, but is under investigation.

One study (109) noted this is also a crucial test of the CKM matrix element V_{tb} : since Γ_t is nearly proportional to $|V_{tb}|^2$,¹³ if V_{tb} were small due to a fourth generation, then top would decay on average after the spin flip time m_t/Λ_{QCD}^2 -

¹³assuming $|V_{tq}| \ll |V_{tb}|$ for $q = d, s$.

the spin correlation would not be seen! This provides the constraint $|V_{tb}| > 0.03$.

4.3 Charge

The electric charge of the top quark has not actually been measured. While it is not widely supposed that its value is not that of the SM, there do exist exotic theories where the top quark is actually much heavier, and the Run 1 observation is of another exotic quark of charge $Q = -4/3$ (117). Techniques to measure this directly at hadron colliders have been explored using the sample of single lepton events that contain a hard photon (118): $t\bar{t} \rightarrow \gamma\ell\nu bj\bar{j}\bar{b}$ (j is a jet from $W \rightarrow q_1\bar{q}_2$).

The photon can be radiated from any electrically charged particle in the process, which means that contributions arise from radiation in top production (including quark initial states), radiative top decay, and radiative W decay. The contribution of radiative W decay is SM-like and its influence can be removed by requiring that the invariant mass of the $jj\gamma$ system and the transverse mass of the $\ell\gamma\cancel{p}_T$ system be larger than 90 GeV. Events are dominated by photons produced in top production if one imposes the cuts:

$$m(b_{1,2}jj\gamma) > 190 \text{ GeV} , \quad m_T(b_{2,1}\ell\gamma\cancel{p}_T) > 190 \text{ GeV} . \quad (13)$$

At Tevatron energies, photon radiation from the initial state quark pairs (which constitutes about 90% of $t\bar{t}$ events) dominates the cross section, so $Q_t = -4/3$ increases the cross section of this sample by only about 20%. At the LHC, however, where $gg \rightarrow t\bar{t}$ dominates, it is enhanced by a factor 2.6, since the cross section is roughly proportional to Q_t^2 . Radiative decay samples are selected by selectively changing one of the relative symbols for the cuts of Eq. 13. In these cases, the sample cross sections actually decrease if $Q_t = -4/3$, due to interference between radiation from the t , W and b lines.

More useful is to examine the p_T and angular distributions of photons for the three $t\bar{t}\gamma$ samples, which are anomalous in the case of exotic charge assignment. For example the photon is typically closer to the lower-energy b quark. The distributions can be used to perform a χ^2 test to distinguish the $Q_t = +2/3, -4/3$ hypotheses. Q_t for this purpose is treated in the literature as a continuous quantity, rather than discrete, because the strict requirement of a viable EW model is simply that the two partners of an $SU(2)$ doublet differ by one unit of charge. However, the models that allow for this realization are quite strange, so we choose to present results in terms of distinctly separating the two discrete charge assignments. Estimates are that Tevatron Run 2 could confirm $Q_t = +2/3$ at 95% C.L. with about 20 fb^{-1} of data using the photon distributions, while the LHC could do this at 100% C.L. with 10 fb^{-1} . A 500 GeV LC could achieve this as well with $\mathcal{O}(100) \text{ fb}^{-1}$ of data (119).

Alternatively, one can look for a few very clean single lepton $t\bar{t}$ events where either the b jet charge is measured, or the b from the leptonic top decay decays semi-leptonically (118). Since $Q_t = Q_b + Q_\ell$, the latter could work even at the Tevatron if experiments are lucky to see a few clean such events. However, measuring b jet charge is less well explored.

4.4 Gauge couplings

We know via observation of $p\bar{p} \rightarrow t\bar{t} \rightarrow b\bar{b}W^+W^-$ at the expected SM rate, and non-observation of other decays (including radiative QED), that the top quark gauge couplings to g, W^\pm, Z, γ are roughly SM-like. These must now be measured precisely; anomalous coupling analyses are the most appropriate. CP violation in the top sector is normally addressed in this language, via the CP-even and -odd

terms in the effective Lagrangians used.

The motivation for studying anomalous QCD top quark gauge couplings is that they naturally arise in dynamical EW symmetry breaking models such as technicolor or topcolor. They have been explored for the Tevatron (120, 121, 69) and LHC (18, 121) (see also references therein). The effective Lagrangian appears as the SM term plus chromoelectric and chromomagnetic dipole moment terms,

$$\mathcal{L}_{t\bar{t}g} = \bar{t} \left[-g_s \gamma^\mu G_\mu - i \frac{g_s \hat{d}'_t}{2m_t} \sigma^{\mu\nu} \gamma_5 G_{\mu\nu} - \frac{g_s \hat{\mu}'_t}{2m_t} \sigma^{\mu\nu} G_{\mu\nu} \right] t. \quad (14)$$

Both terms flip chirality; the chromomagnetic moment $\hat{\mu}'_t$ is CP-even, and the chromoelectric moment \hat{d}'_t is CP-odd, enabling use of CP-even and -odd observables to separate their effects. Because the CP-even chromomagnetic moment interferes with the SM vertex, observables are potentially sensitive to the sign of the coupling. One calculational detail is that for $gg \rightarrow t\bar{t}$ subprocesses, an additional dimension-5 operator must be introduced to preserve gauge invariance, corresponding to an effective $ggt\bar{t}$ 4-point interaction. There is also a SM loop contribution to the chromomagnetic moment, which depends on the Higgs boson mass. For example, for $M_H = 100$ GeV, this leads to a 2.5% correction to $\sigma_{t\bar{t}}$ at the LHC, which is smaller than the expected measurement uncertainty (121). The same study shows $\mathcal{O}(10 - 20)\%$ changes can occur in models containing two Higgs doublets or additional matter content, such as the MSSM.

Unfortunately, Tevatron studies have shown that these moments lead mostly to overall $t\bar{t}$ rate changes, due to threshold effects dominating the angular distributions. Only for very large values of d'_t, μ'_t might one expect to observe shape changes in such distributions as the top quark emission angle in the center-of-mass

frame, or for dileptonic decays at the Tevatron,

$$\hat{O}_L = \frac{1}{m_t^3 |P|^2} P \cdot (Q_+ \times Q_-) P \cdot (Q_+ - Q_-), \quad (15)$$

where $P(Q_+, Q_-)$ is the momentum vector of the proton(ℓ^+, ℓ^-), also in the CM frame. Even then, the statistics at Run 2 may not be sufficient to explore this with confidence. Furthermore, constraints from $b \rightarrow s\gamma$ on the chromomagnetic moment are already an order of magnitude better than is achievable at Tevatron (121). The prospect for explicit CP-odd observables for the chromoelectric moment is greater, but further study with detector simulation and up-to-date Run 2 expectations is needed. Unfortunately, the literature on $t\bar{t}g$ anomalous couplings contains a wide variety of conventions. For LHC studies this is particularly noticeable: results are extremely difficult to compare, both with each other and with other experimental constraints such as from $b \rightarrow s\gamma$. This should be rectified in the near future, to clarify what exactly can be learned.

At hadron colliders, anomalous $t\bar{t}\gamma$ and $t\bar{t}Z$ couplings can be explored only via associated production, as EW s-channel contributions to top pairs are far too suppressed relative to QCD. Up-to-date predictions for these SM rates may be found in Refs. (118, 122). No anomalous coupling analysis for these cases has yet been performed, beyond the top charge measurement of the former. At a LC, these can be studied in direct $t\bar{t}$ production quite precisely (119, 99).

Anomalous $t\bar{t}W$ couplings have been explored for hadron colliders in the context of $t\bar{t}$ production and decay (112), and more recently of single top production (70, 69, 18). For $t\bar{t}$ production the previously discussed limit on right-handed W bosons in top decay is part of this subject, but not normally discussed in

anomalous coupling language. The effective Lagrangian is

$$\mathcal{L} = \frac{gV_{tb}}{\sqrt{2}} \left[W_{\mu}^{-} \bar{b} \gamma_{\mu} P_{-} t - \frac{1}{2M_W} W_{\mu\nu}^{-} \bar{b} \sigma^{\mu\nu} (F_2^L P_{-} + F_2^R P_{+}) t \right] + h.c. \quad (16)$$

where $W_{\mu\nu}^{\pm}$ is the field strength tensor and $P_{\pm} = (1 \pm \gamma_5)/2$; $F_2^{L,R} = 0$ in the SM. The non-SM term is proportional to the particle momentum, and is realized by an anomalous contribution to the cross section at high p_T . In practice one uses the W , b , or bb systems, depending on which single top production component is isolated. Even with 2 fb^{-1} at the Tevatron, limits of approximately $-0.18 < F_2^L < +0.55$ and $-0.24 < F_2^R < +0.25$ could be achieved, assuming a 10% systematic uncertainty. At the LHC this would improve by a factor of 2-3. It is important that this theoretical study be followed up by one with detector simulation to include systematic uncertainties, which will likely be limiting. Limits from a LC would be better by up to an order of magnitude. As a final note, Ref. (123) pointed out that CLEO data on $b \rightarrow s\gamma$ is already more constraining on right-handed tbW couplings than would be achievable at any planned future colliders.

4.5 Lifetime and V_{tb}

The CKM matrix element V_{tb} is intimately related to the top quark lifetime, so it is natural to discuss them together, even though they are often treated as separate topics. We usually speak of the lifetimes of quarks (charm and bottom) and leptons (muon and tau), rather than their intrinsic widths, because they are some fraction of a second that is measureable in the laboratory. Indeed it is such “long” lifetimes that allow high resolution vertex detectors to see the displaced decay vertices of τ leptons, b and c quarks in collider experiments. Like the other fermions, top decays only weakly, so does it also have a long life? Fortunately, no! The top quark lives about 4×10^{-25} s, almost an order of magnitude more

fleeting than the time it takes for a colored particle to hadronize.

A particle's lifetime is the inverse of its decay width, $\tau = \frac{\hbar}{\Gamma}$. In fact we calculated the top lifetime by first calculating its decay width. For extremely short-lived states, it's more useful to discuss the width, rather than the lifetime.

Ignoring the b quark mass, at LO the top quark bW partial width is

$$\Gamma(t \rightarrow Wb) = \frac{G_F}{8\pi\sqrt{2}} m_t^3 |V_{tb}|^2 \left(1 - 3 \frac{M_W^4}{m_t^4} + 2 \frac{M_W^6}{m_t^6} \right) = 1.56 \text{ GeV} . \quad (17)$$

The NLO result is 1.42 GeV (124). Note that the NLO value cannot be used in a LO matrix element calculation - it will give the wrong $\mathcal{B}(t \rightarrow bW)$, because the other couplings are at LO! This partial width is proportional to $|V_{tb}|^2$, just as the other SM decays, $t \rightarrow sW, dW$, are proportional to $|V_{ts}|^2, |V_{td}|^2$, respectively. These are a $\approx 0.2\%$ correction to the total width, $\Gamma_t = \sum_q \Gamma_{tq}$, if there are indeed only 3 generations of quarks, for which case $0.9990 < |V_{tb}| < 0.9993$. We can be confident that $|V_{tb}| \gg |V_{ts}|, |V_{td}|$ even without the low energy unitarity constraints, from the CDF measurement (125)

$$\frac{\mathcal{B}(t \rightarrow bW)}{\mathcal{B}(t \rightarrow qW)} = \frac{|V_{tb}|^2}{|V_{tb}|^2 + |V_{ts}|^2 + |V_{td}|^2} = 0.94_{-0.24}^{+0.31} , \quad (18)$$

which looks for the fraction of tagged b jets in $t\bar{t}$ decays.

It is interesting to consider what happens if there are more than three generations, in which case unitarity constraints on V_{tb} from low energy data are virtually meaningless. From EW precision data we know the rho parameter quite precisely. For four generations its value is (126)

$$\rho \simeq 1 + \frac{3G_F}{8\sqrt{2}\pi^2} \left[m_t^2 |V_{tb}|^2 + m_{t'}^2 |V_{t'b}|^2 \right] = 1 + \frac{3G_F}{8\sqrt{2}\pi^2} \left[m_t^2 + \epsilon^2 (m_{t'}^2 - m_t^2) \right], \quad (19)$$

where t' is the up-type fourth-generation quark, and unitarity in the fourth generation requires that $|V_{tb}|^2 = 1 - \epsilon^2$, $|V_{t'b}|^2 = \epsilon^2$ (given our belief in very small

V_{ts}, V_{td}). It is obvious that either ϵ is small or the top quark and the fourth generation up-type quark are nearly degenerate. The latter case would be discovered quite soon, the fourth generation issue is not one of great concern.

For unstable particles, the width exhibits itself as a spread in the invariant mass distribution of the decay products, the Breit-Wigner lineshape. Unfortunately, the top quark width is narrower than experimental resolution at a hadron collider, so neither Tevatron nor LHC will be able to determine this directly. (One can set limits of the detector resolution, but this will never be competitive with \mathcal{B} checks and other methods.) But determining it is not impossible: one resorts instead to an indirect method of combining several other results which depends on Γ_t . This requires observation of both $t\bar{t}$ and single-top production (in at least one of the three channels) and some mild theoretical assumptions that can be checked, within limits, via detailed studies of decay angular distributions. One has to assume that QCD governs the $t\bar{t}$ production and that the $t\bar{b}W$ vertex is the standard $SU(2)_L$ weak gauge vertex; both are eminently reasonable, and can be checked via anomalous couplings analyses we discussed earlier, which look for deviations in various differential distributions and so are not reliant on only the total rate. All the necessary cross sections are known at NLO or better.

The measurement is linked to $|V_{tb}|$, discussed previously. First, measure $\sigma_{t\bar{t}} \times (\mathcal{B}(t \rightarrow bW))^2$; given trust in QCD and the NLO+NNLL rates, this yields $\mathcal{B}(t \rightarrow bW)$ to 5% at Tevatron Run 2 and 3% at the LHC. Second, measure the SM rate of single-top production, which is really $\sigma_{tX} \times \mathcal{B}(t \rightarrow bW)$. The production cross section, which is proportional to the partial width $\Gamma(t \rightarrow bW)$, is obtained by dividing out the known \mathcal{B} . This is really a measurement of $g_W \times |V_{tb}|$. Assuming exact dependence on the SM gauge coupling g_W , this directly determines $|V_{tb}|$ -

to 12% at the Tevatron (2 fb^{-1}), and 5% at the LHC, where the measurement will be systematics limited. The top quark total width is then the partial width, given by Eq. 17, divided by \mathcal{B} . Precision will be similar to that for the partial width to bW .

For the total width measurement it is expected that the three-generation value of $|V_{tb}|$ would be used, as it is known much more precisely from low energy data than can be measured directly. The technique to measure $|V_{tb}|$ directly at hadron colliders simply establishes to a high degree of confidence that no fourth generation exists, which is already highly disfavored by EW precision data. One may also cross-check $\mathcal{B}(t \rightarrow bW)$ by taking the ratio of dilepton to single lepton events in $t\bar{t}$ production.

4.6 Yukawa coupling

Yukawa couplings relate the matter content of the SM to the source of mass generation, the Higgs sector. For the top quark in the SM this is written as a Lagrangian term $\mathcal{L} = -Y_t \bar{t}_L \phi t_R + h.c.$. When the Higgs field ϕ acquires a vacuum expectation value (vev) v , $\phi \rightarrow \frac{1}{\sqrt{2}}(v + H)$, the vev term becomes the mass and the field term $-\frac{1}{\sqrt{2}}Y_t \bar{t}_L H t_R$ becomes the interaction of a pair of top quarks with the physical Higgs boson. Thus, the top quark mass is fundamentally related to the Higgs vev and its Yukawa coupling, $m_t = \frac{Y_t v}{\sqrt{2}}$. Since $v = 246 \text{ GeV}$ and $m_t = 174.3 \text{ GeV}$, it appears that Y_t is exactly 1, a theoretically interesting value, leading to speculation that important new physics may be accessed via top quark studies. The task then is to verify this, by probing the Higgs-top interaction and therefore the mechanism of fermion mass generation. This turns out to be the most difficult top quark property to measure!

There are three methods to consider at hadron colliders: inclusive Higgs production $gg \rightarrow H$, mediated dominantly by a top quark loop; or associated production with a single top quark, or a pair. Of these, $gg \rightarrow H$ has the largest cross section, but is only minimally useful. First, there is the possibility that additional undiscovered particles mediate a loop contribution, which may not be separable. Second, in 2HDM scenarios, the bottom quark contribution introduces an additional uncertainty since it must be separated. While this channel is still useful, direct access to Y_t via top quark associated production is more attractive.

One would expect the cross section for tH production to be larger than that for $t\bar{t}H$, which is more than two orders of magnitude smaller than $gg \rightarrow H$ due to phase space suppression, since there is more phase space available with only one top quark. Unfortunately, this is not the case, due to a unitarity cancellation between tH diagrams (127), rendering this channel useless. It was hoped that at the Tevatron $t\bar{t}H; H \rightarrow b\bar{b}$ could be observed for a light Higgs, due to the highly unique final state (128). However, the unexpectedly large, negative QCD NLO corrections (129) have all but quashed this hope. At the LHC $t\bar{t}H; H \rightarrow b\bar{b}$ is probably visible for a very light Higgs (130), and it would be possible to observe $t\bar{t}H; H \rightarrow W^+W^-$ for Higgs masses larger than about 120 GeV (122, 131). The statistical uncertainty on Y_t for the latter could be as small as 10%, but the systematics have not been estimated.

At hadron colliders, simply measuring any of these production rates is not sufficient to measure Y_t , despite the commonly held belief that $t\bar{t}H$ grants “direct access” to the top Yukawa coupling. The cross section is a convolution of Y_t and the Higgs branching ratio, which is a priori unknown. Only by multiple Higgs measurements that determine all the Higgs branching ratios can such a cross

section measurement be meaningful. Thus, this aspect of top quark physics is inextricably linked to Higgs physics. At the LHC, where a Higgs signal would not be so statistically limited and would appear in multiple channels, branching ratios can be determined indirectly with mild theoretical assumptions (132), making interpretation of the rates useful. However, an unbiased measurement of Y_t will almost certainly require additional Higgs data from a LC. There is an important corollary to this, for the case of a large excess of events: even if the branching ratio to the observed final state is assumed to be unity, strong constraints can be put on models where Y_t is significantly enhanced over SM expectations. This can happen e.g. in topcolor assisted technicolor models (133).

5 Summary

Discovery of the top quark has opened up a rich field of physics that is justifiably attracting much attention. Careful examination of its production and decay characteristics, and precision measurement of its mass and other properties, are needed to test the SM. Theoretical and experimental efforts towards must proceed hand-in-hand to this end. The top quark may itself lead to the discovery of new physics: the large top mass may well indicate a special role in electroweak and flavor symmetry breakings, and particles yet unobserved may show up in the production or decay of the top. It is also important to understand top quark events as fully as possible, because they will constitute a strong background to many potential new physics signals in other searches.

For the next 5 years or so, direct studies of the top quark belongs to the ongoing Run 2 of the Tevatron. While collider upgrades have resulted in higher rate of production through increases in energy (resulting in a cross-section enhancement

of about 40% for pairs and 60% for single top, compared to Run 1) and integrated luminosity (50 times or more), detector upgrades will allow superior background suppression. We expect that data samples containing $\mathcal{O}(100)$ times as many top quarks as presently available will be collected during this period. After that, the LHC will dominate the field, delivering another factor of $\mathcal{O}(100)$ increase in top quark yield. Better understanding of QCD dynamics is required to make full use of the rich statistics of top events at hadron colliders, leaving plenty of room for work to prepare for the LHC era. High energy physicists around the world have started planning for a future e^+e^- linear collider, which may become operational around 2015. Such a machine will offer new means for precision studies of the top quark properties and dynamics.

In closing, we quote an observant colleague (134), “In physics, one discovery often leads to others. Top opens a new world – the domain of a very heavy fermion – in which the strange and wonderful may greet us.”

Acknowledgement

The authors would like to thank the following people for invaluable advice: Jerry Blazey, Arnd Brandenburg, Tom Ferbel, Mark Kruse, Eric Laenen, Michelangelo Mangano, Steve Martin, Carlo Oleari, Lynne Orr, Stephen Parke, John Parsons, Rob Roser, Zack Sullivan, and Scott Willenbrock. DC’s work was supported in part by a grant from the U.S. National Science Foundation, and JK’s by the U.S. Department of Energy. DR would like to thank Fermilab and DESY, where parts of this work were completed.

Literature Cited

1. Abe F, et al. (CDF Collaboration), *Phys. Rev. D* 50:2966 (1994); *Phys. Rev. Lett.* 74:2626 (1995); Abachi S, et al. (DØ Collaboration), *Phys. Rev. Lett.* 74:2632 (1995).
2. Abazov VM, et al. (DØ Collaboration), *Phys. Rev. D* 67:012004 (2003); Affolder T, et al. (CDF Collaboration), *Phys. Rev. D* 64:032002 (2001); Abe F, et al. (CDF Collaboration), *Phys. Rev. Lett.* 80:2773 (1998); Abachi S, et al. (DØ Collaboration), *Phys. Rev. D* 58:05200 (1998); Abe F, et al. (CDF Collaboration), *Phys. Rev. Lett.* 79:3585 (1997); Abachi S, et al. (DØ Collaboration), *Phys. Rev. Lett.* 79:1203 (1997).
3. Abe F, et al. (CDF Collaboration), *Phys. Rev. D* 59:092001, (1999).
4. Abachi S, et al. (DØ Collaboration), *Phys. Rev. Lett.* 79:1197 (1997); Abbott B, et al. (DØ Collaboration), *Phys. Rev. D* 58:052001 (1998);
5. Estrada J, (DØ Collaboration), arXiv:hep-ex/0302031.
6. Abbott B, et al. (DØ Collaboration), *Phys. Rev. Lett.* 80:2063 (1998); *Phys. Rev. D* 60:052001 (1999).
7. Demortier L, et al. (CDF and DØ Collaborations), Fermilab-TM-2084 (1999).
8. Abe F, et al. (CDF Collaboration), *Phys. Rev. Lett.* 80:2676 (1998); *Phys. Rev. Lett.* 80:2767 (1998); *Phys. Rev. Lett.* 80:2779 (1998); *Phys. Rev. Lett.* 82:271 (1999); *Phys. Rev. Lett.* 82:2808(E) (1999).
9. Affolder T, et al. (CDF Collaboration), *Phys. Rev. Lett.* 84:216 (2000).
10. Abbott B, et al. (DØ Collaboration), *Phys. Rev. Lett.* 85:256 (2000).
11. Affolder T, et al. (CDF Collaboration), *Phys. Rev. D* 65:91102 (2002).
12. Abbott B, et al. (DØ Collaboration), *Phys. Lett. B* 517:282 (2001).
13. Abbott B, et al. (DØ Collaboration), *Phys. Rev. Lett.* 82:4975 (1999); Abazov VM, et al. (DØ Collaboration), *Phys. Rev. Lett.* 88:151803 (2002).
14. Abe F, et al. (CDF Collaboration), *Phys. Rev. Lett.* 79:4975 (1997); Affolder T, et al. (CDF Collaboration), *Phys. Rev. D* 62:012004 (2000).
15. Abe F, et al. (CDF Collaboration), *Phys. Rev. Lett.* 80:2525 (1998).
16. Hagiwara K, et al. (Particle Data Group), *Phys. Rev. D* 66:010001 (2002), <http://pdg.lbl.gov/>.

17. Kane GL, "Top Quark Physics", UM-TH-91-32.
18. Beneke M, et al. "Top quark physics", arXiv:hep-ph/0003033.
19. Abe F, et al. (CDF Collaboration), *Nucl. Instrum. Methods Phys. Res., Sect. A* 271:387 (1988); *Nucl. Instrum. Methods Phys. Res., Sect. A* 350:73 (1994); Abachi S, et al. (DØ Collaboration), *Nucl. Instrum. Methods Phys. Res., Sect. A* 338:185 (1994).
20. Newman-Holmes C (CDF Collaboration), Fermilab-Conf-96/218-E (1996); Blair R, et al. (CDF Collaboration), Fermilab-Conf-96/390-E (1996); Abachi S, et al. (DØ Collaboration), Fermilab-Pub-96/357-E (1996).
21. "ATLAS Detector and Physics Performance Technical Design Report", The ATLAS Collaboration, CERN/LHCC 99-14/15 (1999); "CMS Letter of Intent", CERN/LHCC 92-3(1992)90; Iashvili I, et al., CMS TN/92-34(1992).
22. Bhat PC, Prosper HB, Snyder SS, Fermilab-Pub-98/236 (1998), arXiv:hep-ex/9809011.
23. Wimpenny SJ, Winer BL, *Ann. Rev. Nucl. Part. Sci.* 46:149 (1996).
24. Campagnari C, Franklin M, *Rev. Mod. Phys.* 69:137 (1997).
25. Bernreuther W, et al., arXiv:hep-ph/0111346.
26. Bonciani R, et al. *Nucl. Phys. B* 529:424 (1998).
27. Kidonakis MN, et al. *Phys. Rev. D* 64:114001 (2001).
28. Catani S, et al. *Phys. Lett. B* 378:329 (1996).
29. Beenakker W, et al. *Nucl. Phys. B* 411:343 (1994).
30. Sjöstrand T, *Comp. Phys. Comm.* 82:74 (1994).
31. Marchesini G, et al. *Comp. Phys. Comm.* 67:465 (1992); Corcella G, et al. *JHEP* 0101:10 (2001).
32. Paige FE, Protopopescu SD, *BNL-29777*; Baer H, et al. ISAJET 7.48, arXiv:hep-ph/0001086.
33. Mrenna S, Yuan C-P, *Phys. Rev. D* 55:120 (1997).
34. Orr LH, Stelzer T, Stirling WJ, *Phys. Rev. D* 56:446 (1997).
35. Frixione S, et al. *Phys. Lett. B* 351:555 (1995).
36. Barger VD, Phillips RJ, "Collider Physics," Addison-Wesley (1987).
37. Barnett RM, Hall LJ, arXiv:hep-ph/9609313.
38. Sullivan Z, "Supersymmetric QCD correction to top quark production at the Tevatron,"

1996 DPF Summer Study on New Directions for High-Energy Physics, Snowmass, Colorado,
25 Jun - 12 Jul 1996.

39. Smith MC, Willenbrock S, *Phys. Rev. D* 54:6696 (1996).
40. Mrenna S, Yuan C-P, *Phys. Lett. B* 416:200 (1998).
41. Harris BW, et al. *Phys. Rev. D* 66:054024 (2002).
42. Maltoni F, Sullivan Z, Willenbrock S, arXiv:hep-ph/0301033; Plehn T, *Phys. Rev. D* 67:014018 (2003).and references therein.
43. Stelzer T, Sullivan Z, Willenbrock S, *Phys. Rev. D* 58:094021 (1998).
44. Bordes G, van Eijk B, *Nucl. Phys. B* 435:23 (1995).
45. T. Stelzer, Z. Sullivan and S. Willenbrock, *Phys. rev. D* 56:5919 (1997).
46. Tait T, Yuan C-P, arXiv:hep-ph/9710372.
47. Heinson AP, Belyaev AS, Boos EE, *Phys. Rev. D* 56:3114, (1997); Tait T, *Phys. Rev. D* 61:034001 (2000); Belyaev AS, Boos EE, hep-ph/0003260; Belyaev AS, Boos EE, Dudko LV, *Phys. Rev. D* 59:075001 (1999).
48. Lane K, hep-ph/9501260
49. Eichten E, Lane K, *Phys. Lett. B* 327:129 (1994).
50. Hill CT, Parke SJ, *Phys. Rev. D* 49:4454 (1994).
51. Harris RM, Hill CT, Parke SJ, arXiv:hep-ph/9911288.
52. Casalbuoni R, et al, arXiv:hep-ph/9505212.
53. Holdom B, Ramana MV, *Phys. Lett. B* 353:295 (1995).
54. Popovic MB, Simmons EH, hep-ph/0001302.
55. Appelquist T, Cheng H, Dobrescu B, arXiv:hep-ph/0012100. Appelquist T, Triantaphyllou G, *Phys. Rev. Lett.* 69:2750 (1992).
56. Cho PL, Simmons EH, *Phys. Rev. D* 51:2360 (1995).
57. Atwood D, Kagan A, Rizzo TG, *Phys. Rev. D* 52:6264 (1995).
58. Eichten E, Lane KD, Peskin ME, *Phys. Rev. Lett.* 50:811 (1983).
59. Lane KD, and Eichten E, *Phys. Lett. B* 352:382 (1995).
60. Hill CT, *Phys. Lett. B* 266:419 (1991).
61. Hill CT, *Phys. Lett.* B345:483 (1995).Balaji B, *Phys. Lett.* B393:89 (1997).
62. Simmons EH, *Phys. Rev. D* 55:494 (1997).

63. Affolder T, et al., (CDF Collaboration), *Phys. Rev. Lett.* 85:2062 (2000). Affolder T, et al., (CDF Collaboration), *Phys. Rev. Lett.* 87:102001 (2001).
64. Jain S, (For the DØ Collaboration), arXiv:hep-ex/0302037.
65. Abe F, et al., (CDF Collaboration), *Phys. Rev. D* 59:092001 (1999).
66. CDF, private communication
67. Carlson DO, Yuan C-P, *Phys. Lett. B* 306:386 (1993).
68. Carlson DO, Malkawi E, Yuan C-P, *Phys. Lett. B* 337:145 (1994).
69. Hikasa KI, et al. *Phys. Rev. D* 58:114003 (1998).
70. Boos EE, Dudko LV, Ohl T, production,” *Eur. Phys. J. C* 11:473 (1999).
71. Atwood D, et al. *Phys. Rev. D* 54:5412 (1996).
72. Li CS, et al. *Phys. Rev. D* 57:2009 (1998).
73. Li CS, et al. *Phys. Lett. B* 398:298 (1997).
74. Bar-Shalom S, Atwood D, Soni A, *Phys. Rev. D* 57:1495 (1998).
75. Malkawi E, Tait T, Yuan C-P, *Phys. Lett. B* 385:304 (1996).
76. Oakes RJ, et al. *Phys. Rev. D* 57:534 (1998).
77. Han T, et al. *Phys. Rev. D* 58:073008 (1998).
78. Glashow SL, Iliopoulos J, Maiani L, *Phys. Rev. D* 2:1285 (1970).
79. Peccei R, Zhang X, *Nucl. Phys.* B337:269 (1990); Kane G, Yuan C-P, Ladinsky D, *Phys. Rev. D* 45:124 (1992); Jezabek M, Kuhn JH, *Phys. Lett.* B329:317 (1994); Nelson CA, et al., *Phys. Rev. D* 56:5928 (1997).
80. Dalitz RH, and Goldstein GR, *Proc. R. Soc. Lond. A* 445:2803 (1999).
81. Affolder T, et al. (CDF Collaboration), *Phys. Rev. Lett.* 86:3233 (2001).
82. “Recent Results on Top Quark and Electroweak Physics from CDF”, Lake Louise Winter Institute (2003).
83. Mahlon G, Parke S, *Phys. Lett.* B347:394 (1995).
84. Yue C, et al. *Phys. Rev. D* 64:095004 (2001); Diaz-Cruz JL, et al. *Phys. Rev. D* 41:891 (1990); Eilam G, Hewett J, Soni A. *Phys. Rev. D* 44:1473 (1991).
85. Frey R, et al., arXiv:hep-ph/9704243 (1997); Aguilar-Saavedra JA, Branco GC, *Phys. Lett.* B495:347 (2000).
86. Gunion JF, et al. *The Higgs Hunter’s Guide*, Addison-Wesley (1990).

87. ALEPH, DELPHI, L3, and OPAL Collaborations, LEP Higgs working group (LHWG) note 2001-04, arXiv:hep-ex/0107030.
88. ALEPH, DELPHI, L3, and OPAL Collaborations, LEP Higgs working group (LHWG) note 2001-05, arXiv:hep-ex/0107031.
89. Alam MS, et al., The CLEO Collaboration, *Phys. Rev. Lett.* 74:2885 (1995).
90. Carena M, et al., “Report of the Tevatron Higgs Working Group”, arXiv:hep-ph/0010338.
91. Luke M, and Savage, MJ, *Phys. Lett.* B307:387 (1993).
92. Diaz-Cruz JL, et al. *Phys. Rev. D* 60:115014 (1999).
93. Hosch M, et al. *Phys. Rev. D* 58:034002 (1998); Mahlon G, Kane GL, *Phys. Rev. D* 55:2779 (1997); Ambrosiano S, et al. *Phys. Rev. D* 54:5395 (1996); Mrenna S, Yan CP, *Phys. Lett.* B367:188 (1996); Sender J, *Phys. Rev. D* 54:3271 (1996); Wells JD, Kane GL, *Phys. Rev. Lett.* 76:869 (1996).
94. Affolder T, et al. (CDF Collaboration), *Phys. Rev. D* 63:091101 (2001).
95. Agashe K, Graesser M, *Phys. Rev. D* 54:4445 (1996); Yang JM, Young B-L, Zhang X, *Phys. Rev. D* 58:055001 (1998); Han T, Magro MB, *Phys. Lett. B* 476:79 (2000); Eilam G, et al. *Phys. Lett. B* 510:227 (2001); Abraham KJ, et al. *Phys. Rev. D* 63:034011 (2001).
96. Weinberg S, *Phys. Rev. D* 19:1277 (1979); Susskind L, *Phys. Rev. D* 20:2619 (1979).
97. Dimopoulos S, Susskind L, *Nucl. Phys.* B155:237 (1979); Eichten E, Lane K, *Phys. Lett.* B90:125 (1980).
98. Applequist T, et al. *Phys. Lett.* B220:223 (1989); Takeuchi T, *Phys. Rev. D* 40:2697 (1989); Miransky VA, Yamawaki K, *Mod. Phys. Lett.* A4:129 (1989); Matumoto K, *Prog. Theor. Phys.* 81:277 (1989); Chivukula RS, Cohen AG, Lane K, *Nucl. Phys.* B343:554 (1990);
99. Aguilar-Saavedra JA, et al. (ECFA/DESY LC Physics Working Group Collaboration), Collider,” arXiv:hep-ph/0106315; Abe T, et al. (American Linear Collider Physics Group) “Linear Collider Physics Resource Book”, <http://www.slac.stanford.edu/grp/th/LCBook/>; Abe K, et al. “Physics at JLC”, <http://lcdev.kek.jp/>.
100. Tollefson K, Varnes EW, *Ann. Rev. Nucl. Part. Sci.* 49:435 (1999).
101. Affolder T, et al. (CDF Collaboration), *Phys. Rev. D* 63:032003 (2001). Affolder T, et al. (CDF Collaboration),
102. Orr LH, Stelzer T, Stirling WJ, *Phys. Rev. D* 56:446 (1997). Orr LH, Stelzer T, Stirling

- WJ, *Phys. Rev. D* 52:124 (1995), arXiv:hep-ph/9412294; Orr LH, Stelzer T, Stirling WJ, *Phys. Lett. B* 354:442 (1995). Orr LH, Andre T, Stelzer T, arXiv:hep-ph/9811424.
103. Abe F, et al. (CDF Collaboration), *Phys. Rev. Lett.* 79:1992 (1997);
104. Kondo K, *J. Phys. Soc. Jap.* 57:4126 (1988); *J. Phys. Soc. Jap.* 60:836 (1991).
105. Abe F, et al., (CDF Collaboration), *Phys. Rev. Lett.* 80:2779 (1998).
106. Kharchilava A,
Phys. Lett. B476:73 (2000).
107. Corcella G, Mangano ML, Seymour MH, *JHEP* 0007:004 (2000).
108. Brandenburg A, Si ZG, Uwer P, *Phys. Lett.* B539:235 (2002).
109. Stelzer T, Willenbrock S, *Phys. Lett.* B374:169 (1996).
110. Mahlon G, Parke S, *Phys. Rev. D* 53:4886 (1996). *Phys. Lett.* B411:173 (1997).
111. Bernreuther W, et al. *Phys. Rev. Lett.* 87:242002 (2001); Bernreuther W, Brandenburg A, Si ZG, *Phys. Lett.* B483:99 (2000).
112. Kane GL, Ladinsky GA, Yuan C-P, *Phys. Rev. D* 45:124 (1992).
113. Nelson CA, *Eur. Phys. J.* C19:323 (2001).
114. Parke S, Shadmi Y, *Phys. Lett.* 387:199 (1996).
115. Mahlon G, Parke S, *Phys. Rev. D* 55:7249 (1997); *Phys. Lett. B* 476:323 (2000).
116. Boos EE, Sherstnev AV, *Phys. Lett. B* 534:97 (2002).
117. Chang D, Chang WF, Ma E, *Phys. Rev. D* 59:091503 (1999).
118. Baur U, Buice M, Orr LH, *Phys. Rev. D* 64:094019 (2001).
119. Abe T, et al., The American Linear Collider Working Group Collaboration, in *Proc. of the APS/DPF/DPB Summer Study on the Future of Particle Physics (Snowmass 2001)* ed. Graf N, arXiv:hep-ex/0106057.
120. Atwood D, Aepli A, Soni A, *Phys. Rev. Lett.* 69:2754 (1992); Atwood D, Kagan A, Rizzo TG, *Phys. Rev. D* 52:6264 (1995); Haberl P, Nachtmann O, Wilch A, *Phys. Rev. D* 53:4875 (1996).
121. Martinez R, Rodriguez JA, *Phys. Rev. D* 65:057301 (2002).
122. Maltoni F, Rainwater D, Willenbrock S, *Phys. Rev. D* 66:034022 (2002).
123. Larios F, Perez MA, Yuan C-P, *Phys. Lett. B* 457:334 (1999).
124. Eilam G, et al. *Phys. Rev. Lett.* 66:3105 (1991); Mehen T, *Phys. Lett. B* 417:353 (1998).

125. Affolder T, et al., (CDF Collaboration), *Phys. Rev. Lett.* 86:3233 (2001).
126. Willenbrock S, arXiv:hep-ph/9709355.
127. Maltoni F, et al. *Phys. Rev. D* 64:094023 (2001).
128. Goldstein J, et al., *Phys. Rev. Lett.* 86:1694 (2001), arXiv:hep-ph/0006311.
129. Beenakker W, et al. *Phys. Rev. Lett.* 87:201805 (2001). Reina L, Dawson S, *Phys. Rev. Lett.* 87:201804 (2001); L. Reina, S. Dawson and D. Wackerath, *Phys. Rev. D* **65**, 053017 (2002); S. Dawson, L. H. Orr, L. Reina and D. Wackerath, arXiv:hep-ph/0211438.
130. Richter-Was E, Sapinski M, *Acta Phys. Polon. B* 30:1001 (1999); Drollinger V, Muller T, Denegri D, CMS-NOTE-2002-006, arXiv:hep-ph/0201249.
131. Kostioukhine V, et al. ATL-PHYS-2002-019.
132. Zeppenfeld D, et al. *Phys. Rev. D* 62:013009 (2000).
133. Leibovich AK, Rainwater D, *Phys. Rev. D* 65:055012 (2002).
134. Quigg C, "Top-ology", *Physics Today* May, 1997, arXiv:hep-ph/9704332.

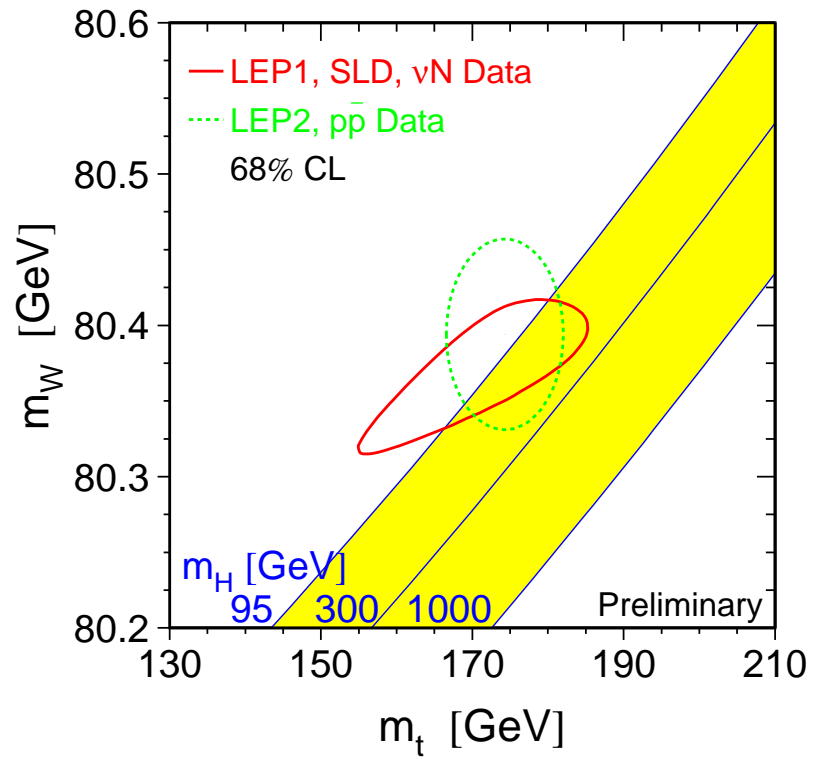


Figure 1: The closed curves representing experimental measurements of M_W and m_t constrain the SM Higgs mass. The shaded band shows the allowed combinations of M_W and m_t for different values of M_H .

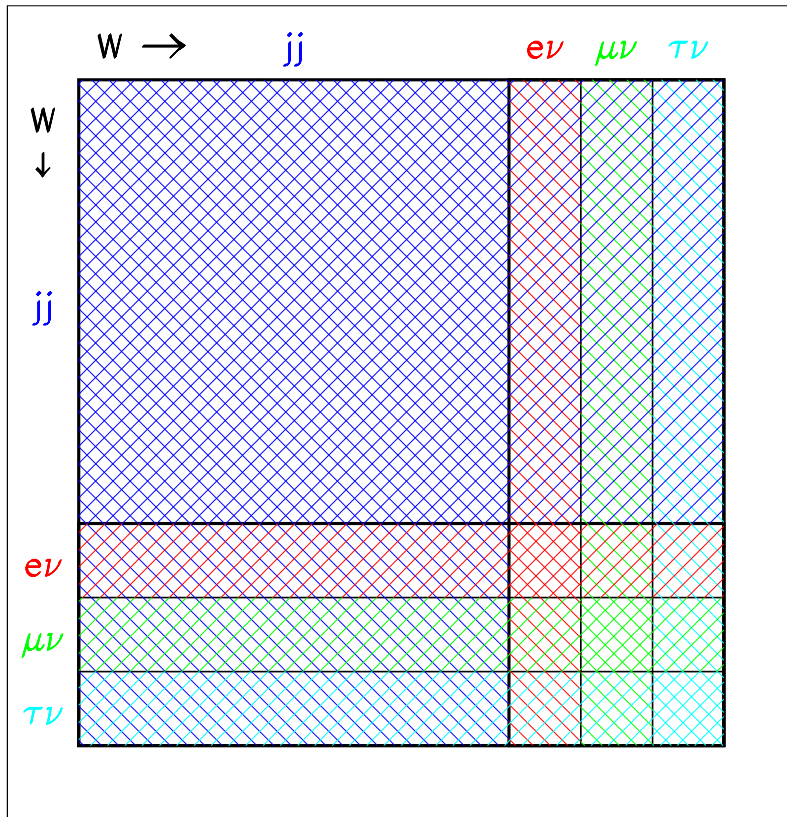


Figure 2: Branching fractions of $t\bar{t}$ due to the various subsequent W decays. All final states have an additional $b\bar{b}$ pair from the top decays.

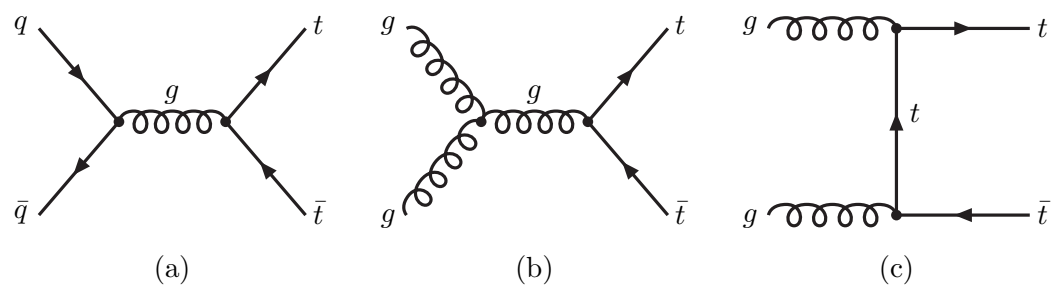


Figure 3: Leading order Feynman diagrams for $t\bar{t}$ production via the strong interaction.

Table 1: Operation parameters of present and future colliders, and cross sections for some important processes. For $\sigma(t\bar{t})$, (a) is the complete NLO+NNLL calculation, while (b) is the partial NNLO+NNLL calculation, discussed in Sec. 2.1.1.

The integrated luminosities are per experiment.

Collider	Tevatron Run 1	Tevatron Run 2	LHC	LC
type	$p\bar{p}$	$p\bar{p}$	pp	e^+e^-
Run period	1992-1996	2001-2008(?)	2007-?	2015(?)-?
E_{CM} (TeV)	1.80	1.96	14.0	$< 2m_t - \sim 1.0$
$\langle \mathcal{L} \rangle$ ($\text{cm}^{-2}\text{s}^{-1}$)	1×10^{31}	1×10^{32}	$10^{33} - 10^{34}$	2×10^{34}
$\int \mathcal{L} dt$ (fb^{-1})	0.125	6.5 - 11	~ 300	~ 1000
σ_{total} (pb)	$\sim 10^{11}$	$\sim 10^{11}$	$\sim 10^{11}$	$\mathcal{O}(10)$
$\sigma(b\bar{b})$ (pb)	$\sim 2 \cdot 10^7$	$\sim 3 \cdot 10^7$	$\sim 3 \cdot 10^8$	$\mathcal{O}(1)$
$\sigma(WX)$ (pb)	$\sim 3 \cdot 10^4$	$\sim 4 \cdot 10^4$	$\sim 2 \cdot 10^5$	$\mathcal{O}(1)$
$\sigma(t\bar{t})(a)$ (pb)	$5.06^{+0.13}_{-0.36}$	$6.97^{+0.15}_{-0.47}$	825^{+58}_{-43}	~ 0.8
$\sigma(t\bar{t})(b)$ (pb)	5.8 ± 0.4	8.0 ± 0.6	-	-
$\sigma(\text{single } t)$ (pb)	1.08 ± 0.01	1.50 ± 0.02	315^{+8}_{-2}	~ 0

Table 2: Single top quark production cross sections (pb).

Process	Tevatron Run 1	Tevatron Run 2	LHC (t)	LHC (\bar{t})
$\sigma_{s\text{-chann}}^{NLO}$	0.380 ± 0.002	0.447 ± 0.002	6.55 ± 0.03	4.07 ± 0.02
$\sigma_{t\text{-chann}}^{NLO}$	0.702 ± 0.003	0.959 ± 0.002	152.6 ± 0.6	90.0 ± 0.5
$\sigma_{\text{assoc.}}^{LL}$	-	0.093 ± 0.024	31^{+8}_{-2}	31^{+8}_{-2}

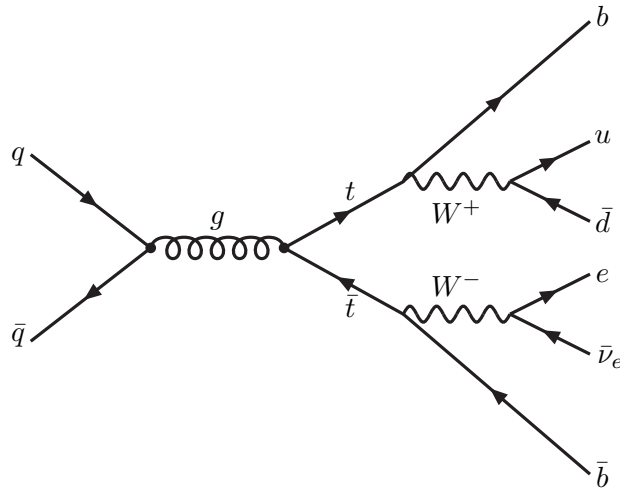
Figure 4: Leading order Feynman diagram of single lepton decay of a $t\bar{t}$ event.

Table 3: Channel-by-channel systematic uncertainties (GeV) in Tevatron Run 1 top mass measurements.

Channel \rightarrow	Dilepton		Single lepton		All-hadronic	
	CDF	DØ	CDF	DØ	CDF	DØ
Jet energy scale	3.8	2.4	4.4	4.0	5.0	?
Model for Signal	2.8	1.7	2.6	1.9	1.8	?
MC generator	0.6	0.0	0.1	0.0	0.8	?
Uranium Noise/Multiple Interactions	0.0	1.3	0.0	1.3	0.0	?
Model for Background	0.3	1.0	1.3	2.5	1.7	?
Method for Mass Fitting	0.7	1.1	0.0	1.5	0.6	?
Total	4.8	3.6	5.3	5.5	5.7	?

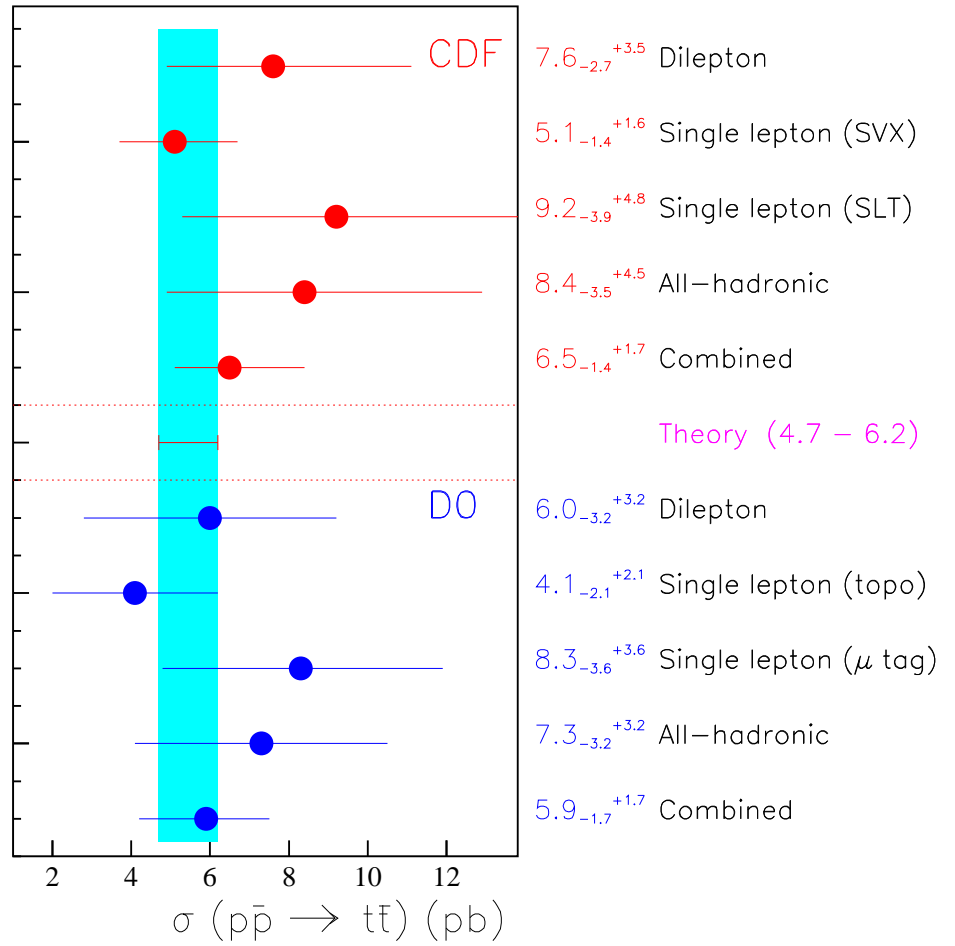


Figure 5: CDF and D0 cross section results for $t\bar{t}$ production at the Fermilab Tevatron, Run 1, overlaid with the theory prediction. For the latter, we take the entire band covered by both the NLO+NLL and partial NNLO+NNLL predictions (see text).

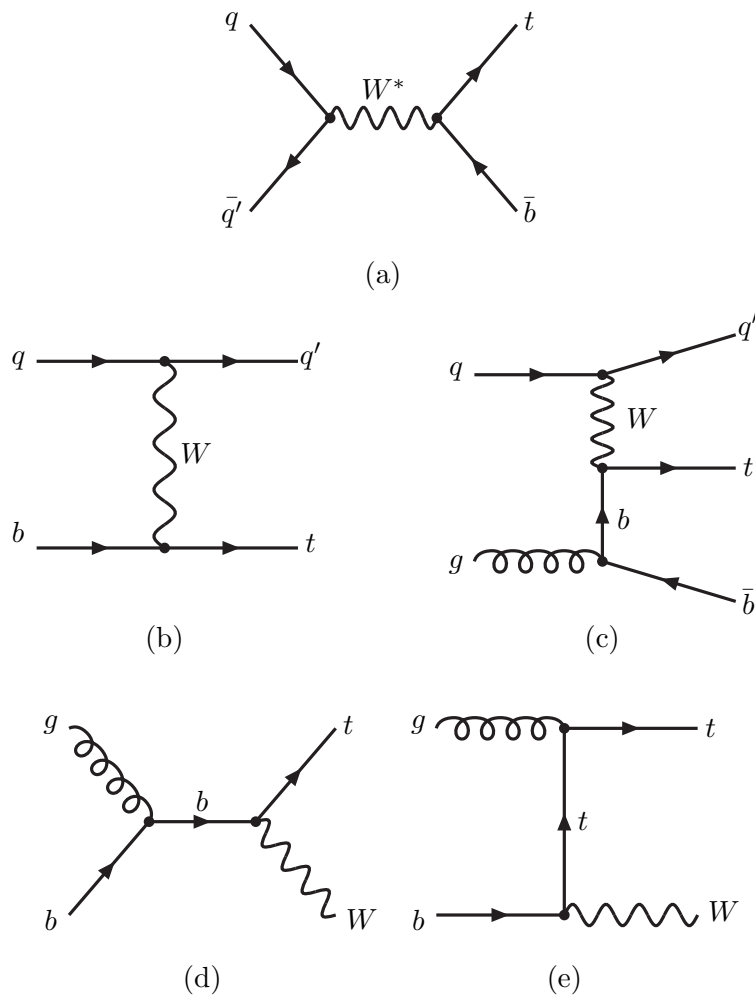


Figure 6: Leading order Feynman diagrams for electroweak production of single top quarks: (a) s -channel, (b,c) t -channel, and (d,e) associated production with a W .

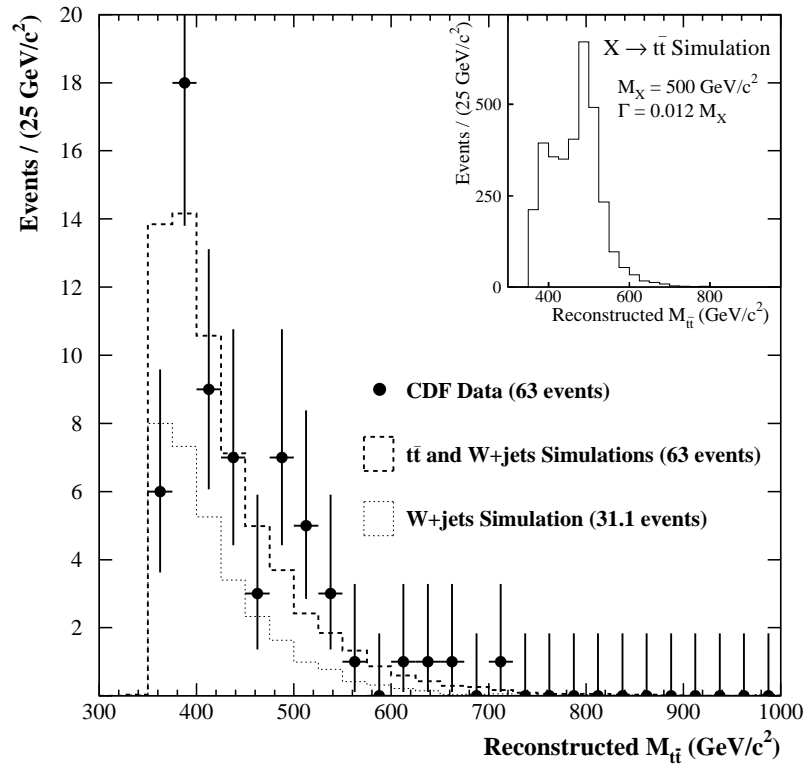


Figure 7: The reconstructed $m_{t\bar{t}}$ distribution in the Run 1 data from the CDF experiment.

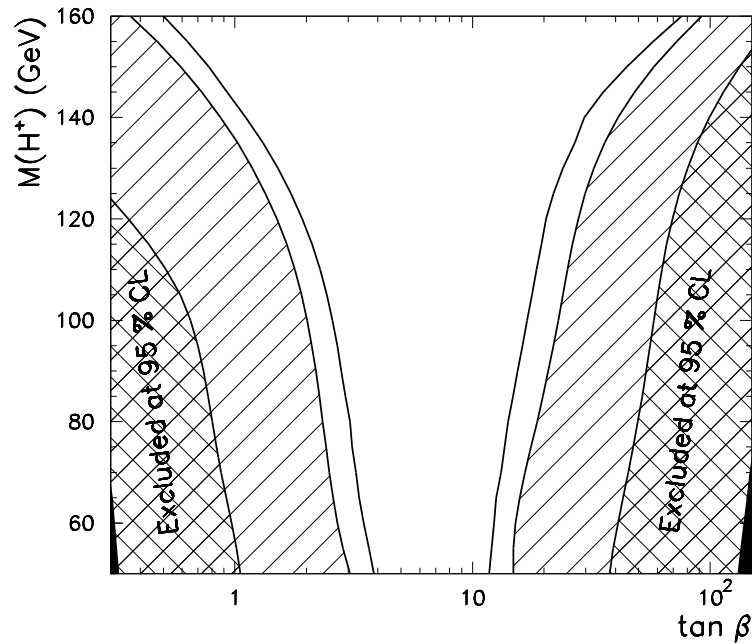


Figure 8: The 95% C.L. exclusion boundaries in the $[M_{H^+}, \tan \beta]$ plane from the DØ Run 1 “disappearance search” for $t \rightarrow bH^\pm$ (double hatched). Also shown are Run 2 projections if the probability of experimental observations continues to peak at the SM prediction: 2 fb^{-1} (single hatched), and 10 fb^{-1} (unhatched). The modeling is based on leading-order calculations. More recent results from LEP have excluded $M_{H^+} < 78.6 \text{ GeV}$ at 95% C.L.

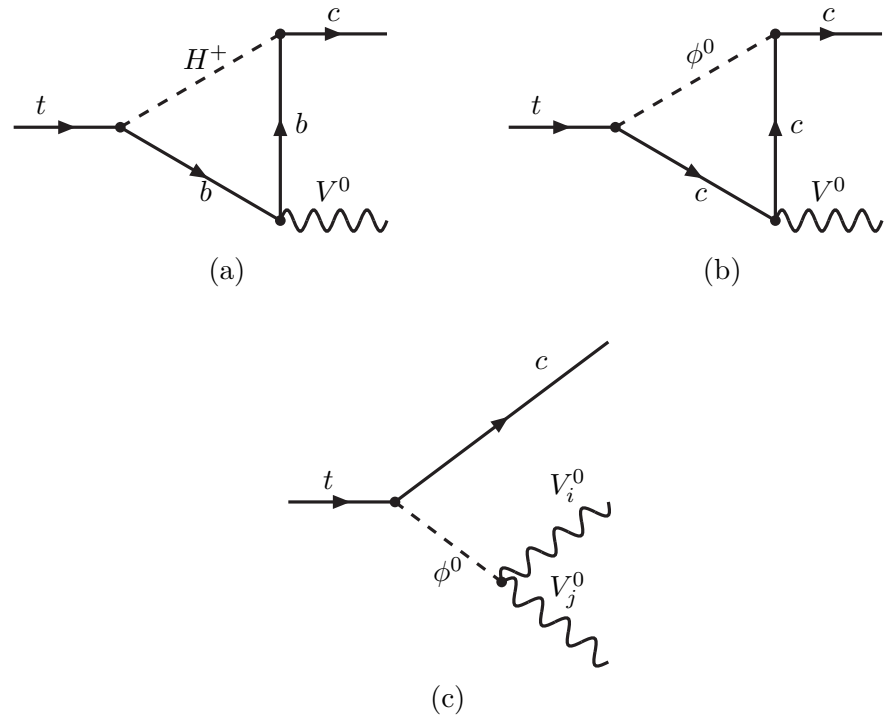


Figure 9: One-loop diagrams of $t \rightarrow cV^0$ (top) and tree diagrams of $t \rightarrow cV_i^0 V_j^0$ (bottom) in 2HDM. $V^0 = \gamma, Z, g$; $\phi^0 = h^0, H^0, A^0$.

Tevatron Top Quark Mass Measurements

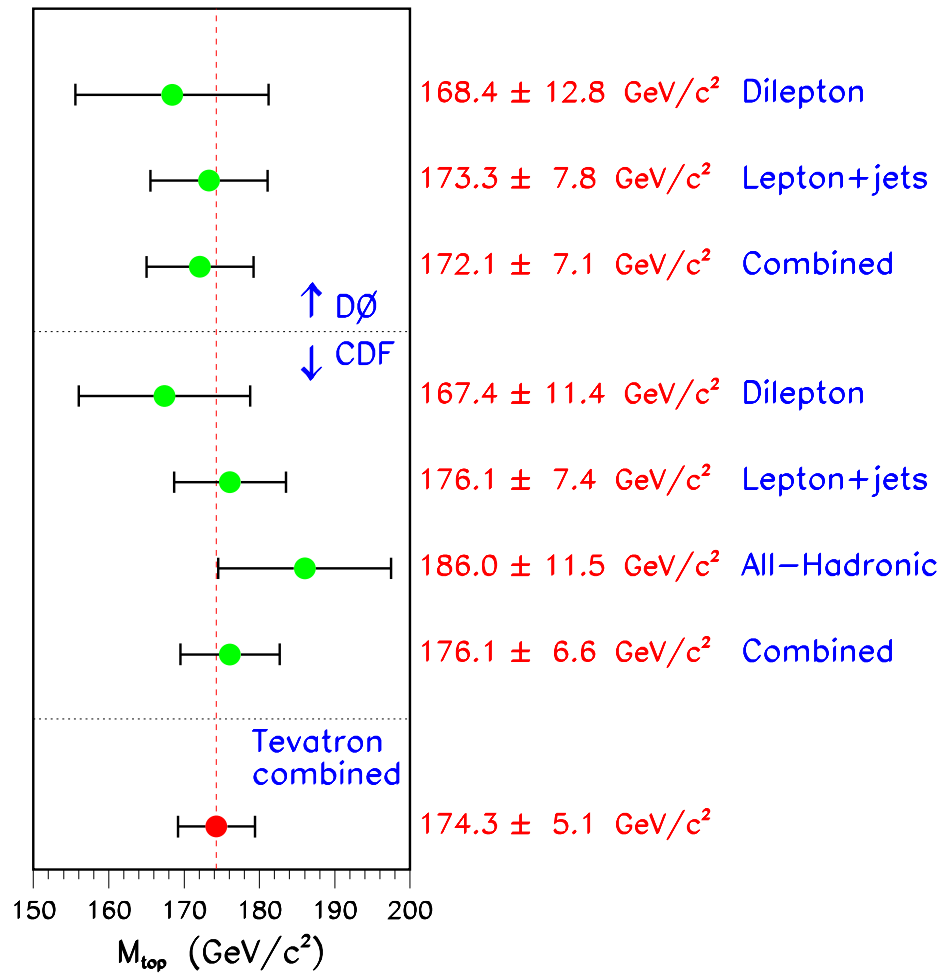


Figure 10: Tevatron results for m_t in the various channels, and the global average.

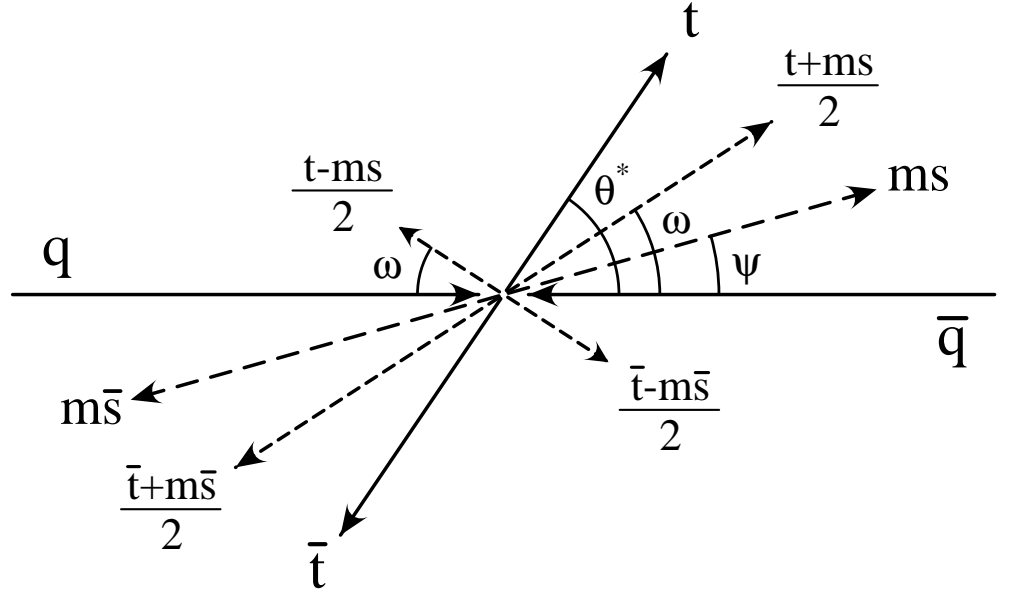


Figure 11: $t\bar{t}$ rest frame (“zero momentum frame”) for $q\bar{q} \rightarrow t\bar{t}$ at hadron colliders, from Ref. (110)(b). $t(\bar{t})$ are the (anti-)top quark momenta, $s(\bar{s})$ are the (anti-)top quark spin vectors. θ^* is the flight direction of the top quark, ψ is the direction of the off-diagonal spin bases, and ω is the preferred emission direction of the down-type fermion in top quark decay for up-down ($t+ms$) and down-up ($t-ms$) spin configurations. All angles are with respect to the p beam direction.